DTIC FILE COPY

②

TECHNICAL REPORT BRL-TR-3121

BRL

AD-A224 885

CURE SIMULATION OF
THICK THERMOSETTING COMPOSITES

DTIC
ELECTE
AUG 0 3 1990
D

TRAVIS A. BOGETTI

JOHN W. GILLESPIE
UNIVERSITY OF DELAWARE

JULY 1990

APPROVED FOR PUBLIC RELEASE; DISTRIBUTION UNLIMITED.

U.S. ARMY LABORATORY COMMAND

BALLISTIC RESEARCH LABORATORY
ABERDEEN PROVING GROUND, MARYLAND

90 08 03 086

NOTICES

REPORT DOCUMENTATION PAGE

Public reporting burden for this collection of information is estimated to average 1 hour per response, including the time for reviewing instructions, searching existing data sources, gathering and maintaining the data needed, and completing and reviewing the collection of information. Send comments regarding this burden estimate or any other aspect of this collection of information, including suggestions for reducing this burden, to Washington Headquarters Services, Directorate for Information Operations and Reports, 1215 Jefferson Davis Highway, Suite 1204, Arlington, VA 22202-4302, and to the Office of Management and Budget, Paperwork Reduction Project (0704-0188), Washington, DC 20503.

1. AGENCY USE ONLY (Leave blank)	2. REPORT DATE	3. REPORT TYPE AND DATES COVERED
	July 1990	Final Jan 89–Apr 90

4. TITLE AND SUBTITLE

Cure Simulation of Thick Thermosetting Composites

5. FUNDING NUMBERS

6. AUTHOR(S)

Travis A. Bogetti
John W. Gillespie, Jr. *

PR: 1L1662618AH80

7. PERFORMING ORGANIZATION NAME(S) AND ADDRESS(ES)

8. PERFORMING ORGANIZATION REPORT NUMBER

9. SPONSORING/MONITORING AGENCY NAME(S) AND ADDRESS(ES)

US Army Ballistic Research Laboratory
ATTN: SLCBR-DD-T
Aberdeen Proving Ground, MD   21005-5066

10. SPONSORING/MONITORING AGENCY REPORT NUMBER

BRL-TR-3121

11. SUPPLEMENTARY NOTES

*   John Gillespie, Jr. is a senior scientist at the Center for Composite Materials and Assistant Professor of Mechanical Engineering, Univ. of Delaware.

12a. DISTRIBUTION/AVAILABILITY STATEMENT

Approved for public release; distribution is unlimited.

12b. DISTRIBUTION CODE

13. ABSTRACT (Maximum 200 words)

The potential for enhanced performance characteristics of composite materials over conventional metals, such as high strength-to-weight ratio, high stiffness, corrosion resistance and low radar signature, makes them extremely attractive for a wide range of military applications. The curing process of thick-section thermosetting composites is critical to the quality and in-service performance of the finished component. In this paper, an investigation into the two-dimensional cure simulation of thick thermosetting composites is presented. Temperature and degree of cure distributions within typical glass/polyester and graphite/epoxy structural elements of arbitrary cross-section (ply-drop and angle bend) are analyzed to provide insight into the non-uniform curing process unique to thick-sections. An incremental, transient finite difference solution scheme is implemented to solve the pertinent governing equations and boundary conditions. Correlation between experimentally measured and predicted through-the-thickness temperature profiles in glass/polyester laminates are presented for various arbitrary temperature cure cycle histories. Spatial gradients in degree of cure are shown to be strongly dependent on part geometry, thermal anisotropy, cure kinetics and the temperature cure cycle. These spatial gradients directly influence the quality and in-service performance of the finished component by inducing warpage and residual stress during the curing process.

14. SUBJECT TERMS

Thermoset Composites; Thick Laminates; Cure Simulation; Anisotropic Heat Conduction; Boundary Fitted Coordinates; Finite Difference Theory

15. NUMBER OF PAGES

62

16. PRICE CODE

17. SECURITY CLASSIFICATION OF REPORT	18. SECURITY CLASSIFICATION OF THIS PAGE	19. SECURITY CLASSIFICATION OF ABSTRACT	20. LIMITATION OF ABSTRACT
UNCLASSIFIED	UNCLASSIFIED	UNCLASSIFIED	SAR

NSN 7540-01-280-5500

Standard Form 298 (Rev 2-89)
Prescribed by ANSI Std Z39-18
298-102

INTENTIONALLY LEFT BLANK.

Contents

List of Figures

List of Tables

INTENTIONALLY LEFT BLANK.

Acknowledgements

INTENTIONALLY LEFT BLANK.

1 Introduction

A fundamental understanding of the relationships between processing and the overall quality and in-service performance of thick-section thermosetting composite structures is needed. The development of residual stresses, for example, is strongly influenced by processing history. Residual stresses can have a significant effect on the mechanics and performance of composite structures by inducing warpage or initiating matrix cracks and delaminations [1,2,3,4,5].

Processing concerns associated with thermosetting composites become increasingly important for components of appreciable thickness [6,7,8]. Perhaps the most familiar concern is an increase in internal temperature resulting from the irreversible exothermic chemical reaction of the matrix phase. Liberated heat is slow to dissipate by conduction and may potentially raise internal part temperatures to levels risking material degradation. A second concern relates to the complex temperature and degree of cure gradients that develop in thick-sections during the curing process [9,10,11]. These gradients induce non-uniform curing within the part that may ultimately lead to a reduction in the overall quality and in-service performance of the finished component. Non-uniform curing can result in incomplete consolidation of the part which, in turn, may lead to undesirable volume fraction gradients and entrapped volatiles or voids [12,13]. Complex cure gradients increase the potential for process-induced warpage and matrix-microcracking and diminished residual properties of the structure.

The objective of this study is to gain a fundamental understanding of the curing process unique to thick thermosetting composites parts of arbitrary cross-section. A two-dimensional anisotropic cure simulation analysis is presented which accounts for thermal and chemical interactions associated with the cure. Several typical glass/polyester and graphite/epoxy structural elements of arbitrary cross-section are analyzed to provide insight into the non-uniform curing process of thick-sections. Spatial gradients in temperature and degree of cure, unique to thick-section composites, are shown to be strongly dependent on part geometry, thermal anisotropy, the chemical cure kinetics and the thermal boundary conditions (cure cycle and tooling). Correlation with experimental measurements of through-the-thickness temperature profiles in glass/polyester laminates are presented

for several arbitrary temperature histories.

2 Background

The autoclave curing process of thermosetting composites has been the subject of numerous investigations [6,12,14,15,16,17]. From early efforts to fabricate thick-section composites, various undesirable effects were encountered that lead to poor part quality. Consequently, most studies have sought to understand the curing process on a fundamental level. Studies of the curing process have focused on the thermal and chemical interactions, degree of cure profiles, viscosity behavior, void formation and growth, and resin flow phenomena occurring in the composite under the application of a specified temperature and pressure cure cycle history [12,13,18]. Other investigations are more empirically oriented, citing general experiences encountered in the fabrication and manufacture of thick-section thermoset composite parts [7,8]. A review of some of the literature associated with the processing of thermosetting composites is now presented. The survey presented here is not intended to be exhaustive, but, those authors cited are felt to have made significant contributions in the area.

Early investigations by Levitsky and Shaffer [9] focused on temperature and degree of cure gradients that develop in chemically reacting isotropic systems. Their one-dimensional analytical solution with prescribed temperature boundary conditions enabled them to investigate the influence of various reaction kinetic variables on the curing process. They extended their work to show the significant influence of temperature and degree of cure gradients on the development of stress in isotropic materials induced by non-uniform curing [19,20,21].

Loos and Springer [12] developed a comprehensive one-dimensional simulation model to describe the curing process of flat plate unidirectional AS4/3501-6 graphite/epoxy composite laminates. The model integrated submodels which describe the fundamental mechanisms associated with the curing process such as the thermo-chemical interactions, resin flow and void formation. Governing equations describing the curing process are solved with an implicit finite difference method. Temperature, degree of cure, resin flow and void size, among other processing variables are predicted as

a function of the autoclave pressure and temperature cure cycle history. Experimental verification of the model was performed and results are in good agreement with simulated predictions.

Kays [6] has conducted a comprehensive three year investigation on the processing issues unique to large area thick-section laminates. The baseline material system was unidirectional AS4/3501 graphite/epoxy. Cure simulation models were developed and used in the investigation. Various autoclave procedures, cure monitoring and non-destructive evaluation (NDE) techniques for thick-section laminates were developed and evaluated. Contributions towards the development of a generic methodology for processing thick-section laminates were made. Interesting observations reported in the study were the development of microcracks and delaminations under certain processing conditions, indicating the importance of processing on the cure and performance of thick-section composites. Although ply-drop geometries were included in the study, cure simulation was limited to a one-dimensional through-the-thickness analysis.

Efforts to optimize cure cycles for the large scale manufacture of thermosetting resin composites have been attempted, [14,16,17]. Computer-aided curing systems, utilizing cure simulation submodels and control feedback systems, were developed. The studies focused on reducing composite manufacturing cost while improving part quality on a reproducible basis.

Bogetti and Gillespie [10] recently conducted a fundamental study of process-induced residual stress in thick-section thermosetting composites. A one-dimensional cure simulation model is coupled to an incremental stress analysis. A constitutive model is proposed to describe 'material behavior during cure that includes chemical hardening, thermal and cure shrinkage effects. Residual stresses are shown to be strongly influenced by gradients in temperature and degree of cure.

While cure simulations models for thermosetting composites are generally based on one-dimensional through-the-thickness assumptions, the cure of arbitrarily shaped thick-sections is significantly influenced by part geometry and anisotropic heat transfer necessitating a two-dimensional analysis. The present investigation contributes to the processing science of thick-section structural elements encountered in the practical application of thermosetting composites. The two-dimensional analysis developed is a prerequisite for studying the evolution of process-induced residual stress and deformation in arbitrarily shaped thick-sections. This work, therefore, represents an important

3

step towards achieving our ultimate goal of building in quality, long life, predictable and reliable performance, durability and lower cycle costs of thick-section thermosetting composite structures for future Army systems.

In the following section the problem formulation is discussed. The governing equations and boundary conditions describing the thermal and chemical interactions associated with the two-dimensional anisotropic curing process are presented. Solution of the pertinent equations utilizing the boundary fitted coordinate system (BFCS) transformation technique in conjunction with the alternating direction explicit (ADE) finite difference method is then described.

3 Analysis

3.1 Assumptions

The analysis assumes that gradients in temperature and degree of cure normal to the cross-section of the part geometry are negligible. This assumption is valid for large area parts where edge effects are minimal. All thermal and cure kinetic material parameters are assumed constant, independent of time and temperature. It is also assumed that no resin flow or part thickness reduction occurs during the curing process. The no-resin flow assumption is reasonable for the large area, net resin or low bleed thermosetting composite systems investigated in this study.

3.2 Heat Conduction Equation

Temperature solutions are based on Fourier's heat conduction equation for two-dimensional, transient anisotropic heat transfer with constant material properties and an internal heat generation source term. The equation is well established and is referenced here for completeness as [22]:

$$\dot{q} + k_{xx}\frac{\partial^2 T}{\partial x^2} + 2k_{xz}\frac{\partial^2 T}{\partial x \partial z} + k_{zz}\frac{\partial^2 T}{\partial z^2} = \rho c_p \frac{\partial T}{\partial t}$$

$$for \quad T(x,z) \quad in \quad \tilde{D} \tag{1}$$

where $\tilde{D}$ is the domain of interest defined in an orthogonal (x, z) coordinate system. The term $\dot{q}$ represents internal heat generation and k_{xx}, k_{zz}, k_{xz} are the effective anisotropic thermal conduc-

4

tivities, ρ is the density, and c_p is specific heat of the composite. T and t are absolute temperature and time, respectively.

The coordinate directions in equation (1) are defined in a fixed (x, z) global coordinate system. Fiber-reinforced composites exhibit anisotropic thermal properties defined in a principle coordinate system with coordinate axes parallel and perpendicular to the fiber direction. Fiber orientation will generally vary with respect to the global coordinate system in an arbitrary shaped geometry. The effective anisotropic thermal conductivities in equation (1) are based on the second order tensor transformation of the principle thermal conductivities given by:

$$
\begin{pmatrix} k_{xx} \\ k_{zz} \\ k_{xz} \end{pmatrix} = \begin{pmatrix} m^2 & n^2 & mn \\ n^2 & m^2 & -mn \\ -mn & mn & m^2 - n^2 \end{pmatrix} \begin{pmatrix} k_{11} \\ k_{33} \\ k_{13} \end{pmatrix}
\tag{2}
$$

In equation (2), $m = cos(\theta), n = sin(\theta)$ and k_{11}, k_{33} and k_{13} are the longitudinal, transverse and cross-term thermal conductivities of the composite in its principle (1,3) material coordinate system, respectively. Fiber orientation within the domain is assumed coincident with the curvilinear coordinate system, (η, ξ), shown in Figure (1). In our simulations, the fiber orientation is coincident with $\eta = $ constant grid lines in the domain. This definition of fiber orientation requires that layers within the laminate conform to the tool surface profile and does not accommodate laminate stacking sequence variations.

The rotation angle, θ, is defined by the local orientation between the fiber direction and the global (x, z) coordinate system. Transformation at a node in the domain is graphically illustrated in Figure (1) where the orientation angle between the principle (1, 3) and global (x, z) coordinate systems is defined.

3.3   Temperature Boundary Conditions

A generalized temperature boundary condition formulation is used to permit flexibility in the simulation of the autoclave curing process. Either Dirichlet, Neumann or Robin boundary conditions may be enforced on the domain boundaries. The generalized boundary condition is expressed
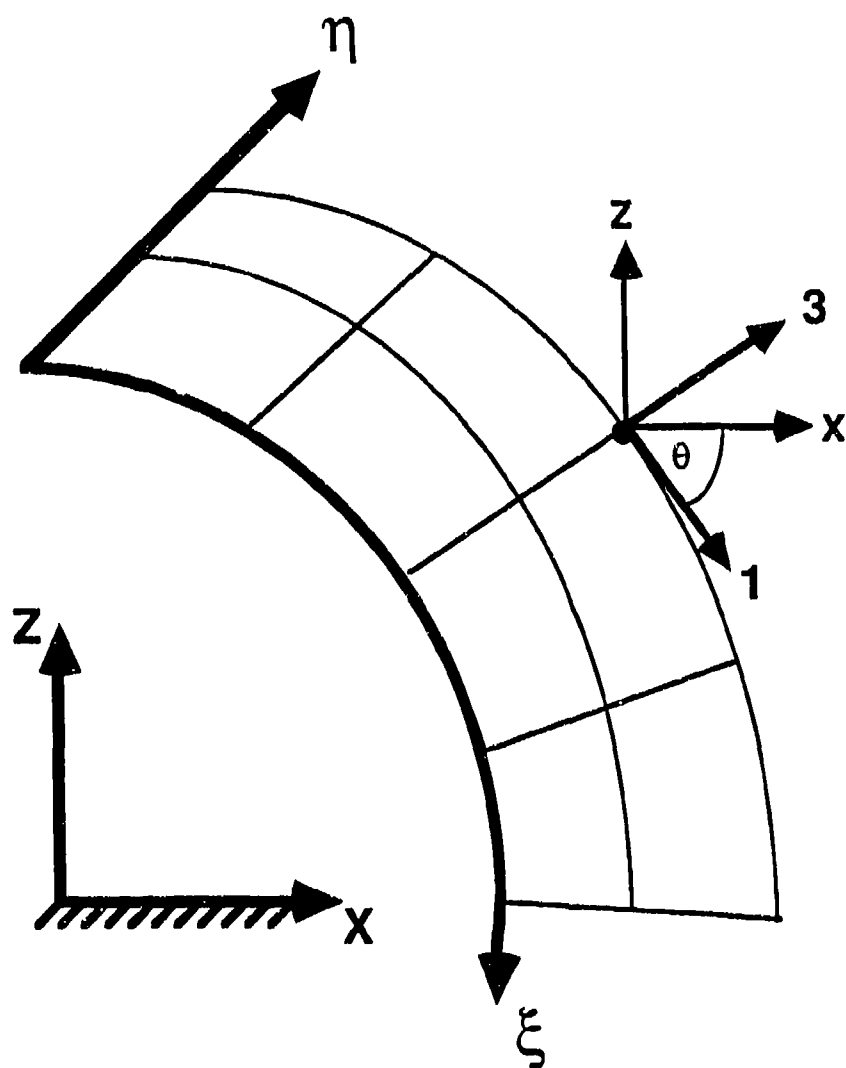
5

Figure 1: Thermal Conductivity Transformation Between Coordinate Systems

mathematically as:

$$a\frac{\partial T_s}{\partial n} + bT_s + c\tilde{T}(t) = 0$$

$$for \quad T(x,z) \quad on \quad \partial\tilde{D} \tag{3}$$

where $\partial\tilde{D}$ represents the domain boundary or part surface. The surface boundary temperature is T_s and $\hat{n}$ is the outward unit normal to the domain surface. The coefficients a, b, and c define the effective heat transfer across the domain boundaries. The expression $\tilde{T}(t)$ in equation (3) is interpreted as either the ambient autoclave temperature cure cycle or the actual boundary surface temperature, depending on the values of a, b and c specified. Table (1) summarizes the three possible boundary conditions obtainable from this generalized formulation.

The Neumann or insulated boundary condition is used when symmetry conditions are imposed to conserve computation time by reducing the number of nodes required for the simulation. The Dirichlet or prescribed temperature boundary condition is most useful when experimental transient part surface temperatures are known. In the presence of tooling or a bag assembly, these temperature profiles are not known apriori and may be very different from the cure cycle. In this case, the Robin boundary condition is used where $(h/k)_{eff}$ defines the effective heat transfer coefficient quantifying the heat flux from the actual part surface to the environment. This effective boundary condition accounts for all thermal resistance associated with the tooling and bag assembly.

3.4 Chemical Kinetics

The term $\dot{q}$ in equation (1) represents the instantaneous heat generation per unit volume of material and is introduced to account for the exothermic chemical reaction associated with the curing process. It is a cure rate dependent term which is evaluated throughout the domain at every time step during the incremental solution.

The degree of cure, α, at a material point is defined as the ratio of the cumulative heat liberated from the chemical reaction, $H(t)$, to the total heat of the reaction, H_r. This is mathematically expressed as:

$$\alpha = \frac{H(t)}{H_r} \tag{4}$$

7

The heat liberated at any point in time, t, is expressed in integral form:

$$H(t) = \int_0^t \frac{1}{\rho}(\frac{dq}{dt})dt \qquad (5)$$

dq/dt is the rate of heat generation from the cure reaction. The total heat of reaction is similarly expressed as:

$$H_r = \int_0^{t_f} \frac{1}{\rho}(\frac{dq}{dt})dt \qquad (6)$$

where t_f is the time for complete reaction. Heat generation at a material point is identically zero for $t \geq t_f$. Equations (4), (5) and (6) are combined to yield an expression for the cure rate:

$$\frac{d\alpha}{dt} = \frac{1}{\rho H_r}(\frac{dq}{dt}) = \frac{1}{\rho H_r}\dot{q} \qquad (7)$$

The cure rate, $d\alpha/dt$, is a time and temperature dependent function of the reacting material system and is typically determined empirically with isothermal Differential Scanning Calorimetry (DSC) techniques. The cure rate is often expressed in terms of time, temperature and degree of cure in some form of the Arrhenius rate equation. Details of the experimental procedures for determining cure rate expressions and the total heat of reaction are found elsewhere [23,24]. Once $d\alpha/dt$ and H_r for the material are known, the heat generation term in equation (1) is straightforwardly obtained by rearrangement of equation (7):

$$\dot{q} = \rho H_r \frac{d\alpha}{dt} \qquad (8)$$

3.5 Initial Conditions

The model formulation is flexible enabling arbitrary initial temperature, T_i, and degree of cure, α_i, distributions throughout the domain at the start of the simulation to be specified. Uniform initial conditions are specified in all simulations presented in this study:

$$T(x,z) := T_i \quad in \quad \tilde{D} \quad at \quad t = 0$$
$$\alpha(x,z) = \alpha_i \quad in \quad \tilde{D} \quad at \quad t = 0 \qquad (9)$$

T_i and α_i are taken to be the ambient temperature and zero, respectively.

8

3.6 Boundary Fitted Coordinate System Transformation Technique

The boundary fitted coordinate system (BFCS) transformation technique is used to solve the governing equation (1) and generalized boundary condition (3). The BFCS technique is a mapping technique in which coordinates in a physical curvilinear coordinate system, (x, z), are transformed into a computational rectangular coordinate system, (ξ, η). Motivation for using the technique in the present investigation is its advantage to easily accommodate complex shaped geometries. Once the governing equations and boundary conditions are transformed into the computational domain, a straightforward finite difference solution technique is applied. Solutions are obtained in the computational domain and subsequently mapped back into the physical domain through the correspondence of nodes in the respective planes. A conceptual representation of the relationship between the two coordinate systems is illustrated in Figure (2), where a one-to-one correspondence between nodes in each coordinate system is noted. The transformation from the physical domain into the computational domain is based on the Poisson equation.

The BFCS technique is well documented [25,26], so derivation and details of the coordinate transformation procedure are omitted for brevity. Utilization of the BFCS technique in this investigation involves both a mesh generation procedure and coordinate transformation of the governing equation (1) and boundary condition (3). All the finite difference meshes presented in this investigation were produced with the mesh generation code TGMESH developed by Gilmore [27].

Transformation of the governing equation (1) through the Poisson equation into the computational domain yields:

$$\dot{q} + A_1\frac{\partial^2 T}{\partial \xi^2} + A_2\frac{\partial^2 T}{\partial \eta^2} + A_3\frac{\partial^2 T}{\partial \xi \partial \eta} + A_4\frac{\partial T}{\partial \xi} + A_5\frac{\partial T}{\partial \eta} = \rho c\frac{\partial T}{\partial t} \tag{10}$$

where the spatial coordinates in the computational domain are ξ and η. Finite difference formulas for the spatial and time derivatives appearing in equation (10) are presented in the Appendix. The coefficients, A_i, are functions of the effective thermal conductivities, k_{xx}, k_{zz} and k_{xz}, and spatial derivatives in the physical domain and are defined in the Appendix.

Transformation of the generalized boundary condition (3) is also required. Details of the transformation procedure are presented elsewhere [28]. Consequently, only the final expressions are

9

Physical Curvilinear Coordinate System

Jacobian
Transformation

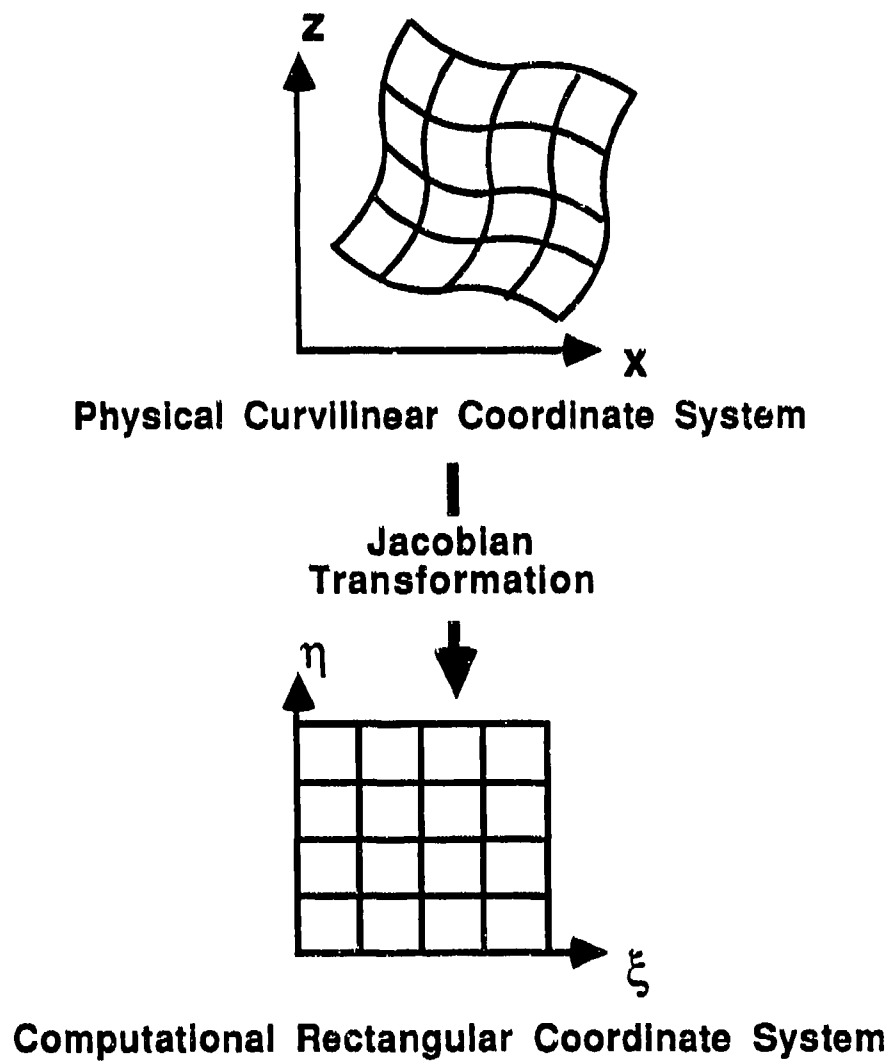**Computational Rectangular Coordinate System**

Figure 2: Conceptual Representation of the Physical and Computational Domains

presented here. Neumann and Robin boundary conditions are functions of the temperature gradient on the domain boundary. The computational domain has four separate faces comprising its entire surface as indicated in Figure (3). Each face or side of the domain has a unique expression for the temperature gradient on the boundary surface, $\partial T_s/\partial \hat{n}$, given by:

$$\frac{\partial T_s}{\partial \hat{n}} = \frac{\alpha T_\xi - \beta T_\eta}{J\sqrt{\alpha}} \quad on \quad the \quad \hat{n}(+\xi) \quad face$$

$$\frac{\partial T_s}{\partial \hat{n}} = \frac{\gamma T_\eta - \beta T_\xi}{J\sqrt{\gamma}} \quad on \quad the \quad \hat{n}(+\eta) \quad face$$

$$\frac{\partial T_s}{\partial \hat{n}} = \frac{\beta T_\eta - \alpha T_\xi}{J\sqrt{\alpha}} \quad on \quad the \quad \hat{n}(-\xi) \quad face \tag{11}$$

$$\frac{\partial T_s}{\partial \hat{n}} = \frac{\beta T_\xi - \gamma T_\eta}{J\sqrt{\gamma}} \quad on \quad the \quad \hat{n}(-\eta) \quad face$$

the coefficients α, β and γ and the Jacobian coordinate transformation, J, are functions of the spatial derivatives in the physical domain, (x, z), and are defined in the Appendix. Substituting equations (11) into equation (3) yields the expressions for the transformed generalized temperature boundary conditions on each face of the computational domain:

$$a\frac{\alpha T_\xi - \beta T_\eta}{J\sqrt{\alpha}} + bT_s + cT(t) = 0 \quad on \quad the \quad \hat{n}(+\xi) \quad face$$

$$a\frac{\gamma T_\eta - \beta T_\xi}{J\sqrt{\gamma}} + bT_s + cT(t) = 0 \quad on \quad the \quad \hat{n}(+\eta) \quad face$$

$$a\frac{\beta T_\eta - \alpha T_\xi}{J\sqrt{\alpha}} + bT_s + cT(t) = 0 \quad on \quad the \quad \hat{n}(-\xi) \quad face \tag{12}$$

$$a\frac{\beta T_\xi - \gamma T_\eta}{J\sqrt{\gamma}} + bT_s + cT(t) = 0 \quad on \quad the \quad \hat{n}(-\eta) \quad face$$

Transformations on temperature, (i.e. T_s and $T(t)$), are not required since scalars transform identically. Equations (10) and (12) constitute the transformed heat transfer equation and temperature boundary conditions governing the transient temperatures distributions in the composite during the curing process. The solution to the system of resulting finite difference equations is now presented.

3.7 Alternating Direction Explicit Finite Difference Method

The Alternating Direction Explicit (ADE) finite difference method [29] is employed in the solution of equations (10) and (12). The ADE method is preferred over an implicit method because substantial reduction in computation time is realized. The ADE method does not require the inversion of the
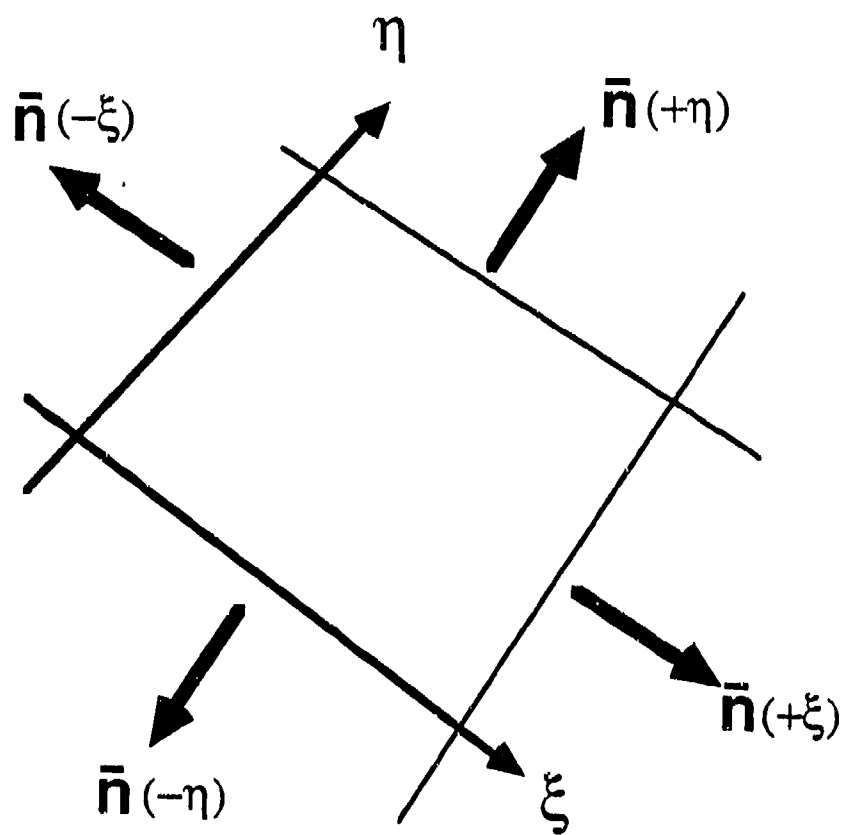
Figure 3: Normal Derivatives on the Computational Domain Boundaries

12

temperature coefficient matrix encountered in the implicit approach. It is also preferred over a fully explicit method since it has been shown to be unconditionally stable with time step size, and is less sensitive to computational errors [29].

The ADE finite difference method applies a fully explicit approach twice on the computational domain for each time step increment. One sweep through the finite difference mesh is made in a systematic forward direction where a pseudo-temperature solution, $u_{i,j}$, at each interior node is defined explicitly in terms of adjacent nodes. For the same time step, another sweep is made in exactly the reverse direction to obtain a second pseudo temperature solution, $v_{i,j}$. The temperature at node i, j, ($T_{i,j}$), is then computed at each interior node for the current time step as the arithmetic average of the two pseudo-temperature solutions:

$$T_{i,j} = \frac{u_{i,j} + v_{i,j}}{2} \tag{13}$$

The computational mesh of nodal dimensions m by n is illustrated in Figure (4). Central differencing formulas are employed at all interior nodes, while forward and backward differencing formulas are used on the boundaries nodes. All finite differencing formulas are documented in the Appendix.

Following the detailed procedure described by Barakat and Clark [29], the expression for $u_{i,j}$ at the time step $t + \Delta t$ for an interior node during a forward sweep is given by:

$$u_{i,j}^{t+\Delta t} = (1/((\rho c_p/\Delta t) + A_1 + A_2))_{i,j} \left[(\rho c_p/\Delta t)_{i,j} u_{i,j}^t + \dot{q}_{i,j}^t + \right.$$

$$(A_1)_{i,j}(u_{i+1,j}^t - u_{i,j}^t + u_{i-1,j}^{t+\Delta t}) + (A_2)_{i,j}(u_{i,j+1}^t - u_{i,j}^t + u_{i,j-1}^{t+\Delta t}) +$$

$$(A_3/4)_{i,j}(u_{i+1,j+1}^t - u_{i+1,j-1}^{t+\Delta t} - u_{i-1,j+1}^t + u_{i-1,j-1}^{t+\Delta t}) +$$

$$\left. (A_4/2)_{i,j}(u_{i+1,j}^t - u_{i-1,j}^{t+\Delta t}) + (A_5/2)_{i,j}(u_{i,j+1}^t - u_{i,j-1}^{t+\Delta t}) \right] \tag{14}$$

The $u_{i,j}$'s at time step $t + \Delta t$ on the right hand side of equation (14) all have previously been computed during that same time step, (i.e. those with subscripts $(i - 1, j)$, $(i, j - 1)$, $(i + 1, j - 1)$ and $(i - 1, j - 1)$). Similarly, $v_{i,j}$ at time step $t + \Delta t$ for an interior node during a backward sweep is given by:

$$v_{i,j}^{t+\Delta t} = (1/((\rho c_p/\Delta t) + A_1 + A_2))_{i,j} \left[(\rho c_p/\Delta t)_{i,j} v_{i,j}^t + \dot{q}_{i,j}^t + \right.$$
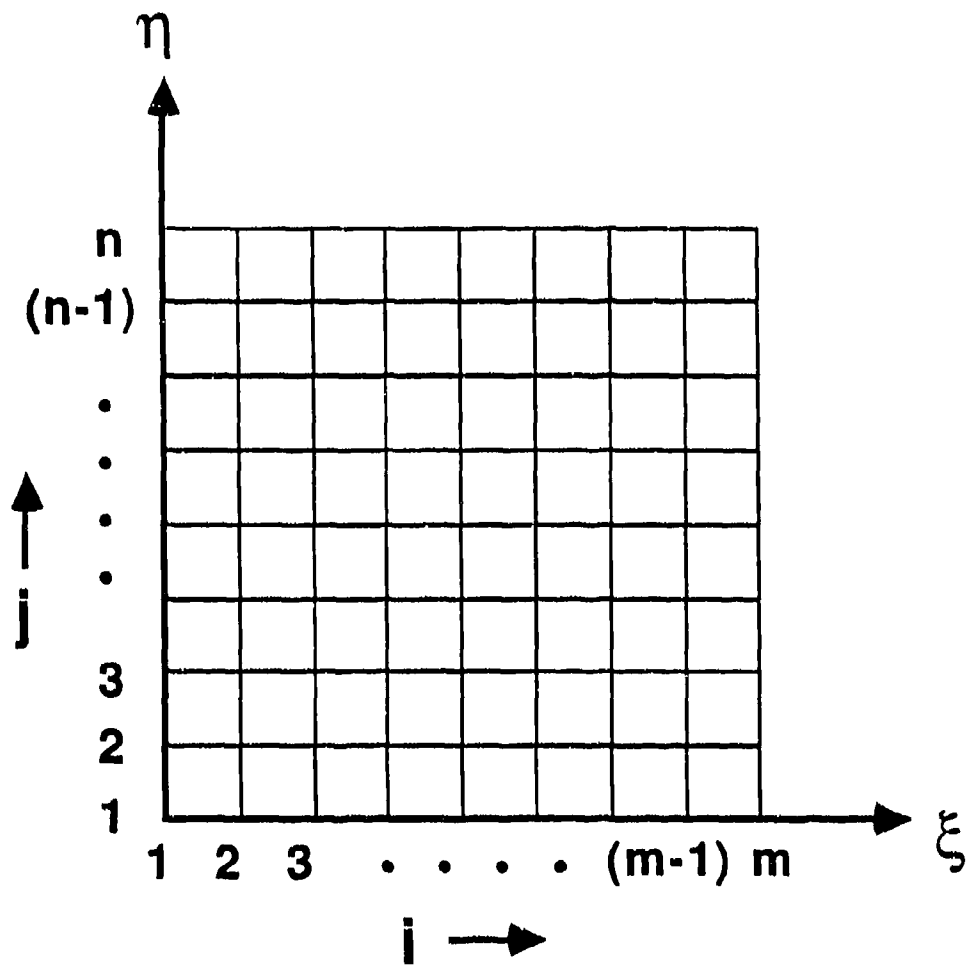
13

Figure 4: The Computational Mesh

$$(A_1)_{i,j}(v_{i+1,j}^{t+\Delta t} - v_{i,j}^t + v_{i-1,j}^t) + (A_2)_{i,j}(v_{i,j+1}^{t+\Delta t} - v_{i,j}^t + v_{i,j-1}^t) +$$

$$(A_3/4)_{i,j}(v_{i+1,j+1}^{t+\Delta t} - v_{i+1,j-1}^t - v_{i-1,j+1}^{t+\Delta t} + v_{i-1,j-1}^t) +$$

$$(A_4/2)_{i,j}(v_{i+1,j}^{t+\Delta t} - v_{i-1,j}^t) + (A_5/2)_{i,j}(v_{i,j+1}^{t+\Delta t} - v_{i,j-1}^t)] \tag{15}$$

where the $v_{i,j}$'s at time step $t + \Delta t$ on the right hand side of equation (15) are those previously computed during the same time step, (i.e. those with subscripts $(i + 1, j), (i, j + 1), (i - 1, j + 1)$ and $(i - 1, j - 1)$).

Boundary nodes are treated in the usual fully explicit fashion since no time derivatives appear in the transformed generalized temperature boundary condition expressions. An explicit representation for the boundary node temperature, T_s, in terms of adjacent nodes is obtained by substitution of the appropriate one-sided three-point differencing formulas presented in the Appendix into the generalized boundary condition equations (12).

The heat generation term, $\dot{q}_{i,j}^t$, in equations (14) and (15), is computed from equation (8), rewritten here as:

$$\dot{q}_{i,j}^t = \rho H_r \left(\frac{d\alpha}{dt}\right)_{i,j}^t \tag{16}$$

where $(d\alpha/dt)_{i,j}^t$ is the instantaneous cure rate at node (i, j) evaluated at time step t. Instantaneous cure rates are computed based on instantaneous temperature and degree of cure through an empirical rate expression. Temperature distributions at time $t + \Delta t$ are obtained by solving the finite difference equations (14) and (15) and substituting into (13) in conjunction with the appropriate explicit representations of the boundary temperatures defined in equation (12).

3.8 Degree of Cure Calculation

The degree of cure over each time step increment during the simulation is based on the degree of cure at the previous time step and the instantaneous cure rate at the current time step. The degree of cure at node (i, j) for time step $t + \Delta t$ is computed from the relationship:

$$\alpha_{i,j}^{t+\Delta t} = \alpha_{i,j}^t + \left(\frac{d\alpha}{dt}\right)_{i,j}^{t+\Delta t} \Delta t \tag{17}$$

15

The value of $\alpha_{i,j}^t$ is known since it was computed at the previous time step increment and $(d\alpha/dt)_{i,j}^{t+\Delta t}$ is also known, from the empirically determined cure rate expression.

Temperature and degree of cure distributions throughout the domain are computed at each time step increment as a function of the cure cycle temperature history. A computer code was written to perform the numerical calculations. Results of this investigation are discussed in the following section.

4   Results and Discussion

The cure simulation analysis developed is used to gain a fundamental understanding of the curing process unique to thick-section composites. A summary of the input is presented first. Verification of the cure simulation analysis is demonstrated by comparison with available exact solutions for simulated temperature and degree of cure profiles. Predicted temperature profiles are compared to experimentally measured values within several 2.54 cm thick glass/polyester laminates exposed to various temperature histories. The influence of the tooling on the curing process is demonstrated through the generalized boundary condition formulation. The influence of laminate thickness and the temperature cure cycle ramp on non-uniform through-the-thickness curing are illustrated to demonstrate the complex curing phenomena unique to thick-section composites. Several typical glass/polyester and graphite/epoxy structural elements of arbitrary cross-section are analyzed to show the strong dependence of temperature and degree of cure gradients on geometry and material thermal anisotropy.

4.1   Input Summary

Required input data for the cure simulation analysis includes; (1) solution details including the boundary and initial conditions, (2) the finite difference mesh representation of the part geometry, (3) thermal properties and (4) a cure kinetic description of the composite material system.

16

4.1.1 Solution Details

The desired cure cycle thermal history, $T(t)$, is segmented into descrete time step increments, Δt. Since the ADE method used in this investigation is unconditionally stable with the time step size, little difficulty in obtaining a converged solution was encountered. In general, time step increments between one and two seconds proved to be sufficiently small to yield converged solutions for all the cure simulation results presented.

The transient temperature boundary conditions for the analysis are based on the specified temperature cure cycle history and the effective heat transfer coefficients a, b and c defined in the generalized boundary condition discussed previously. Initial conditions are defined in equation (9).

4.1.2 Mesh Input

The part geometry is discretized into a suitable finite difference mesh consisting of m by n nodes. The physical (x, z) coordinates of each node in the mesh are used to evaluate the spatial derivatives appearing in transformed governing equations. The finite difference meshes employed in this investigation were generated with a computer software code TGMESH[27] that is based on the BFCS technique. Three geometries typical of structural composite components are used in this investigation; a flat plate, a 90° right angle bend and a ply-drop. The finite difference mesh representations of these geometries are shown in Figure (5). The flat plate and right angle bend geometry are of constant thickness equal to 2.54 cm. The ply-drop geometry consists of a 1.27 cm flat section joined to a 2.54 cm flat section by a sinusoidal transition region. Fiber orientation in each geometry is assumed coincident with the $(\eta = constant)$ grid lines. Solution accuracy is influenced by refinement of the finite difference mesh. Mesh refinement was chosen to yield converged solutions in all the cure simulations performed in this investigation.

4.1.3 Thermal Properties

The thermal properties used in this investigation for the glass/polyester and graphite/epoxy composites are summarized in Table (2). The cross-term thermal conductivity, k_{13}, in the principle
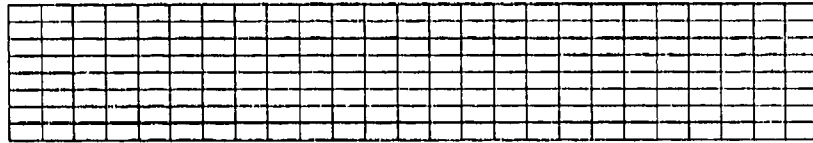
(a) Flat Plate Geometry Mesh
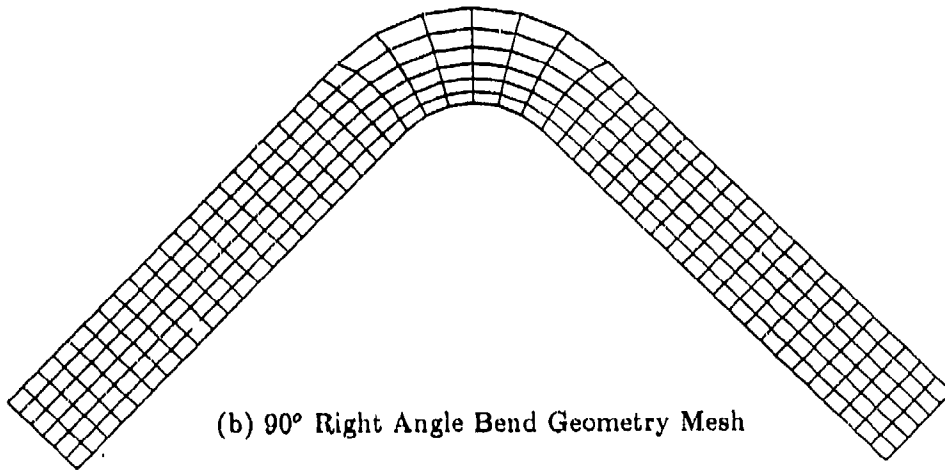
(b) 90° Right Angle Bend Geometry Mesh

(c) Ply-Drop Geometry Mesh

Figure 5: Cure Simulation Mesh Geometries

18

coordinate system of both materials is identically zero.

4.1.4 Cure Kinetic Data

The complete description of the cure kinetics for the composite includes the total heat of reaction and a description of the rate of reaction as a function of temperature and degree of cure. Reaction rate expressions for the glass/polyester and graphite/epoxy material systems are different in form due to the inherent differences in the overall order of the reaction kinetics.

The glass/polyester composite consists of CYCOM 4102 polyester resin, manufactured by the American Cyanamid Corporation, and a woven roving E-glass plain weave fabric reinforcement containing approximately 6 yarns per inch. The reaction rate expression for the glass/polyester system is second-order overall [24]:

$$\frac{d\alpha}{dt} = A_c exp(-\Delta E_c/RT)\alpha^{m_c}(1 - \alpha)^{n_c} \tag{18}$$

R is the universal gas constant and T is absolute temperature. The exponents m_c and n_c, the pre-exponential coefficient, A_c, the activation energy, ΔE_c, and the total heat of reaction are listed in Table (3).

The graphite/epoxy composite contains Hercules Corporation's 3501-6 resin, reinforced with unidirectional AS4 graphite fibers. The reaction rate expression for the graphite/epoxy system follows a markedly different form [12]:

$$\frac{d\alpha}{dt} = (k_1 + k_2\alpha)(1 - \alpha)(0.47 - \alpha) \qquad for \quad (\alpha \le 0.3)$$
$$\frac{d\alpha}{dt} = k_3(1 - \alpha) \qquad for \quad (\alpha > 0.3) \tag{19}$$

k_1, k_2 and k_3 are defined by the Arrhenius rate expressions:

$$k_1 = A_1 exp(-\Delta E_1/RT)$$
$$k_2 = A_2 exp(-\Delta E_2/RT) \tag{20}$$
$$k_3 = A_3 exp(-\Delta E_3/RT)$$

Dirichlet (prescribed)	$a = 0$	$b = 1$	$c = -1$
Neumann (insulated)	$a = 1$	$b = 0$	$c = 0$
Robin (convective)	$a = 1$	$b = (h/k)_{eff}$	$c = -(h/k)_{eff}$

Table 1: Generalized Boundary Condition Coefficients

	ρ [kg/m^3]	c_p [kJ/(W·°C)]	k_{33} [kW/(in · °C)]	k_{11}/k_{33}
Glass/Polyester	1.89×10^3	1.26	2.163×10^{-4}	2
Graphite/Epoxy	1.52×10^3	9.42×10^{-1}	4.457×10^{-4}	1,5,10

Table 2: Thermal Properties for Glass/Polyester and Graphite/Epoxy Composites

Glass/Polyester [24]	
m_c	0.524
n_c	1.476
A_c[min.$^{-1}$]	3.7×10^{22}
ΔE_c[J/mol]	1.674×10^5
H_r[kJ/kg]	77.5
Graphite/Epoxy [12]	
A_1[min.$^{-1}$]	2.102×10^9
A_2[min.$^{-1}$]	-2.014×10^9
A_3[min.$^{-1}$]	1.960×10^5
ΔE_1[J/mol]	8.07×10^4
ΔE_2[J/mol]	7.78×10^4
ΔE_3[J/mol]	5.66×10^4
H_r[kJ/kg]	198.9

Table 3: Cure Kinetic Parameters for Glass/Polyester and Graphite/Epoxy Composites

The pre-exponential coefficients A_1, A_2 and A_3, the activation energies, ΔE_1, ΔE_2 and ΔE_3, and the total heat of reaction for the graphite/epoxy composite are summarized in Table (3).

4.2 Model Verification

Cure simulation results were verified for accuracy by comparing predicted temperature and degree of cure profiles with available exact solutions. Temperature predictions are based on an analytical one-dimensional transient temperature solution [22]. Temperature profiles in a glass/polyester laminate of thickness $\ell=2.54$ cm, initially at 0°C and exposed to constant boundary temperatures of 0°C at $z=0$(bottom surface) and 10°C at $z=\ell$(top surface), were compared at $z=\ell/4$, $z=\ell/2$ and $z=3\ell/4$ locations. The cure simulation mesh utilized is the flat plate geometry illustrated in Figure (5), employing insulated boundary conditions on the sides to isolate one-dimensional heat transfer effects. Excellent agreement with the exact solution is shown in Figure (6), providing confidence in the accuracy of the cure simulation analysis.

Degree of cure profiles obtained from the analysis were compared to independent results based on the cure rate constitutive relations. Degree of cure profiles in a glass/polyester flat laminate under uniform, isothermal conditions are compared in Figure (7). Results are in excellent agreement which confirms the accuracy of this portion of the analysis.

4.3 Experimental Correlation

Experimental temperature distributions within 2.54 cm thick flat plate glass/polyester laminates processed under various arbitrary autoclave temperature cure cycle histories were correlated with the cure simulation predictions. Thermocouples were embedded within the laminates at various locations through the thickness and temperature distributions were monitored during the autoclave cure cycle. The laminates, 15.24 cm by 15.24 cm by 2.54 cm thick in dimension, were constructed by stacking together approximately 42 plys of prepreg. The assembly was placed on a 0.635 cm thick aluminum caul plate, topped with a single layer of bleeder cloth and surrounded by an aluminum dam to prevent transverse resin flow and compaction. The entire assembly was placed within a vacuum bag, sealed to the caul plate with tacky tape and drawn to one atmosphere of vacuum pressure.
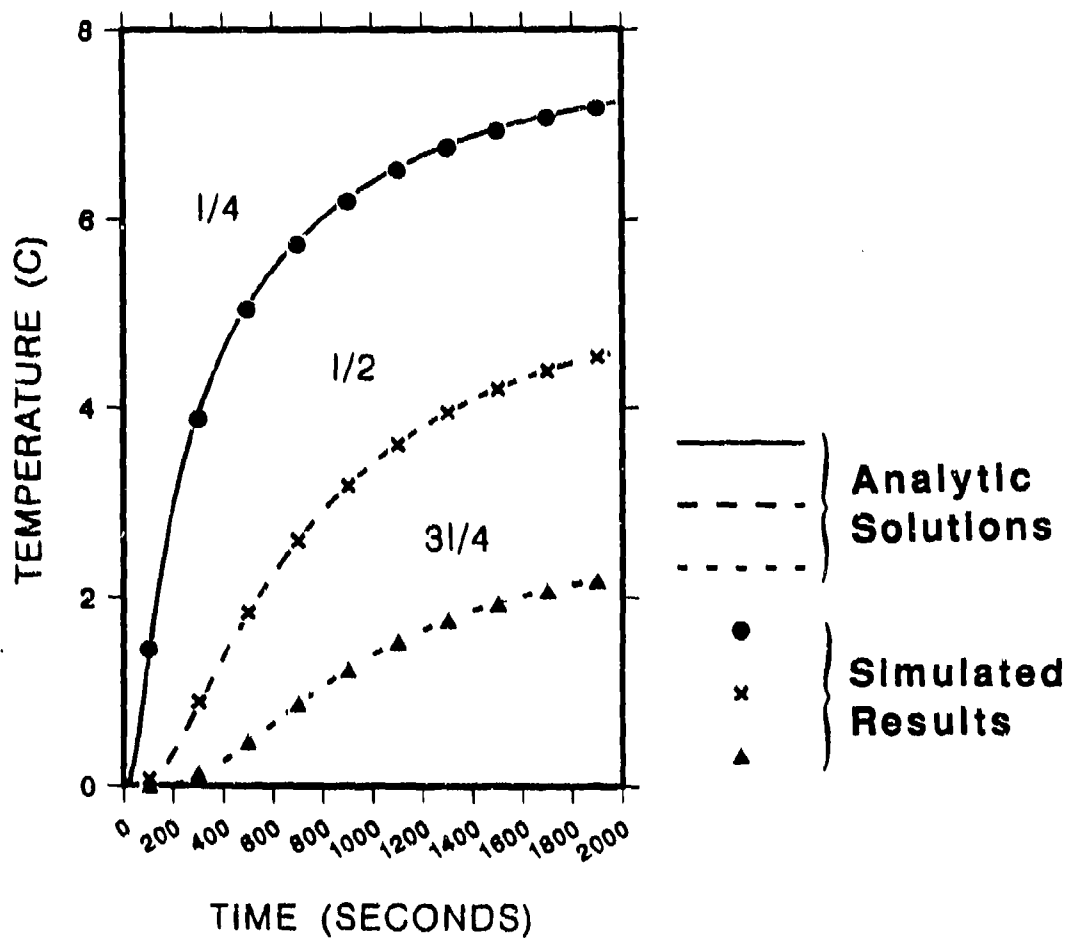
21

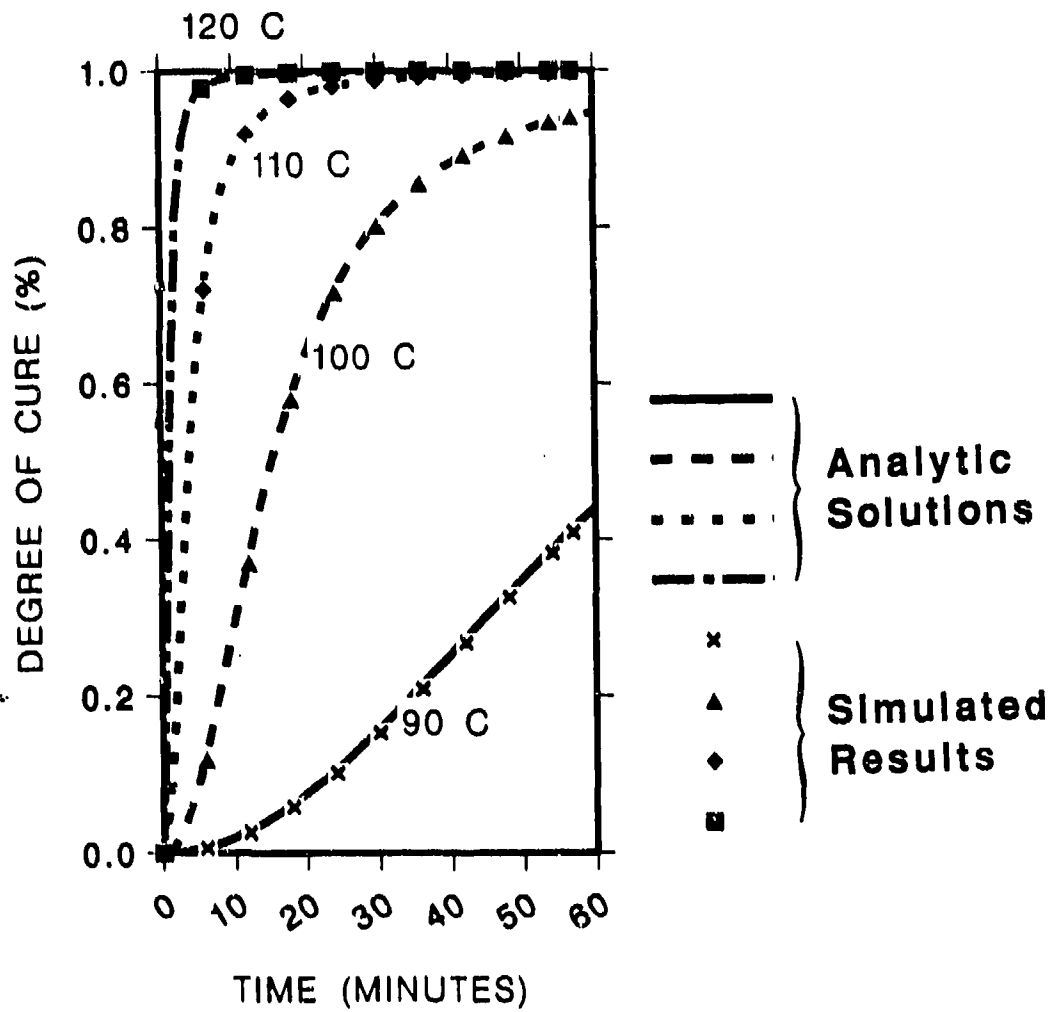Figure 6: Verification of Temperature Solution in a Glass/Polyester Laminate

22

Figure 7: Verification of the Degree of Cure Solution in a Glass/Polyester Laminate

The laminates were then placed into the autoclave and subjected to various prescribed temperature cure cycle histories. During the cure, temperature profiles at the various locations within the laminate were monitored with an IBM personal computer linked to a KEITHLEY data aquisition system. Thermocouple readings were sampled every 30 seconds to ensure accurate temperature measurements during points in the cure cycle when large temperature gradients develop.

The thermal properties and cure kinetic input data presented previously for the glass/polyester system and the flat plate mesh geometry were used in the correlation. A parametric study identified the effective heat transfer coefficient, $(h/k)_{eff}$, to be 87[1/m] on the top surface and 125[1/m] on the bottom surface of the laminate assembly in contact with the aluminum tool surface. In addition, insulated boundary conditions were employed on the sides to isolate through the thickness effects. Comparison of numerical and experimental transient temperature profiles at the center of the laminates subjected to three different cure cycles are presented in Figures (8), (9) and (10). Good agreement in this experimental study offers additional independent validation of the cure simulation analysis.

4.4 Boundary Condition Effects

The presence of the tooling, bag assembly and the internal autoclave environment can profoundly influence the heat transfer to the composite and may ultimately alter the curing process within the part. The net effect is that the surface temperature variation of the part may be significantly different than the prescribed cure cycle temperature. While convective heat transfer due to heat flow within the autoclave is not modeled explicitly, flexibility with the generalized boundary condition formulation enables the influence of the effective heat transfer to the part on the curing process to be investigated. In the limit as $(h/k)_{eff} \to \infty$, the actual surface temperature of the part approaches the prescribed cure cycle temperature, $T(t)$. As $(h/k)_{eff} \to 0$, an insulated boundary condition is approached. The generalized boundary condition formulation enables the influence of various tools and bagging assemblies on the curing process to be investigated.

The following example demonstrates the influence $(h/k)_{eff}$, can have on the curing process. A 2.54 cm thick glass/polyester laminate was subjected to cure cycle temperature history indicated
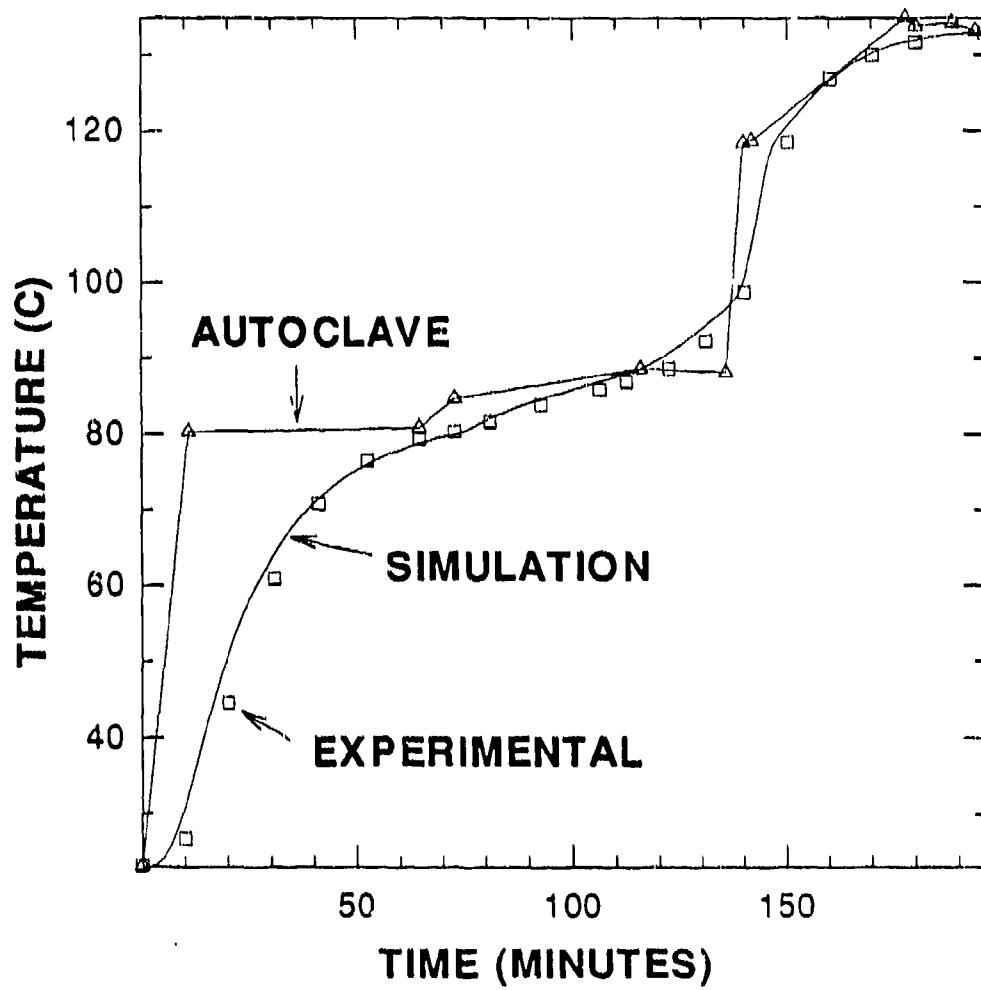
24

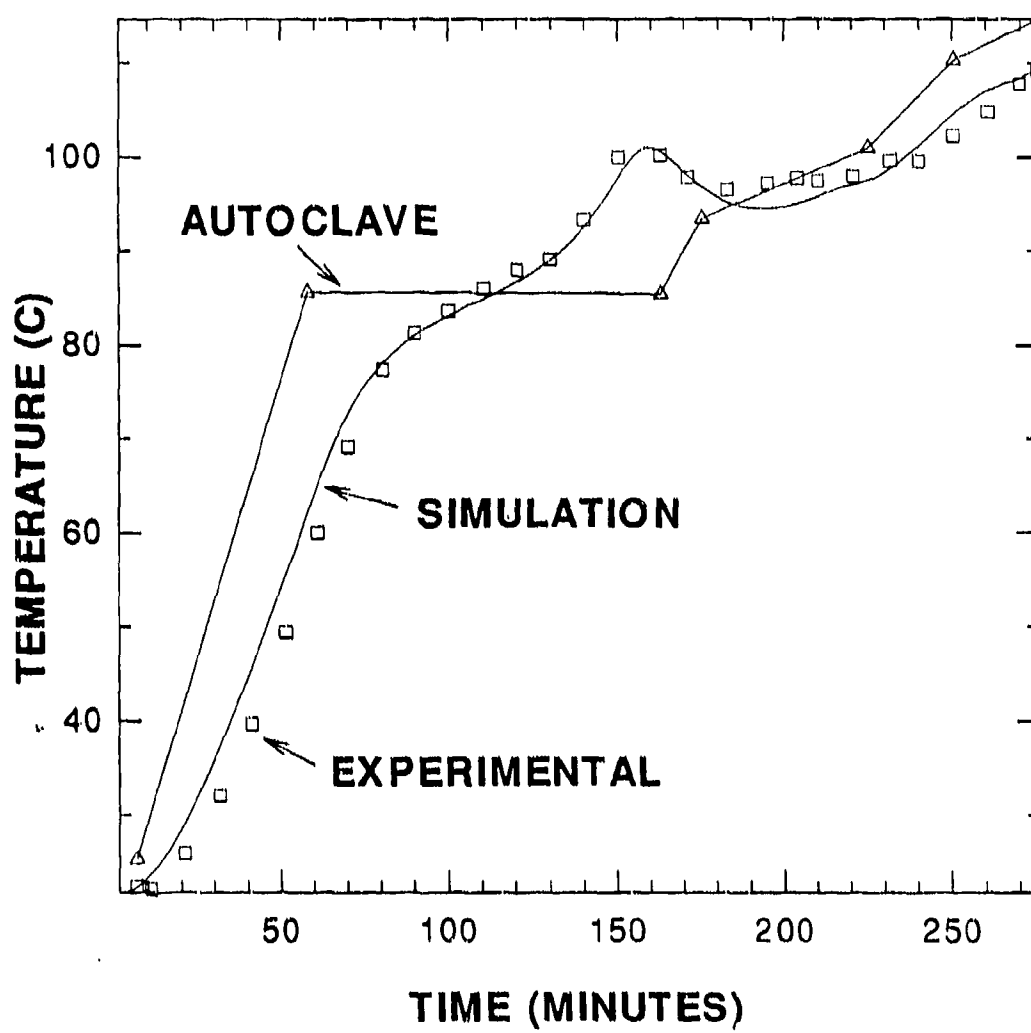Figure 8: Temperature Comparision with Glass/Polyester Laminate 1

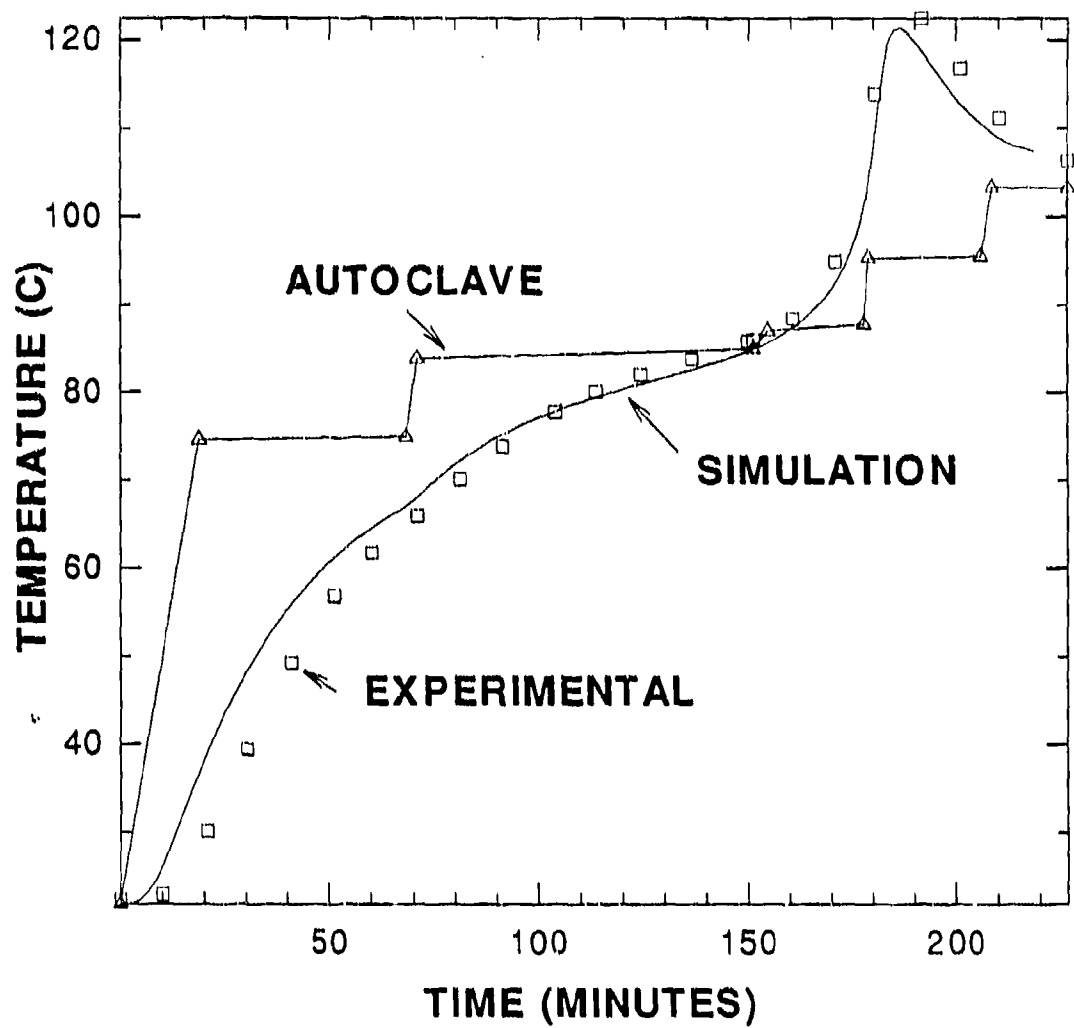Figure 9: Temperature Comparison with Glass/Polyester Laminate 2

Figure 10: Temperature Comparison with Glass/Polyester Laminate 3

27

in Figure (11) with specified $(h/k)_{eff}$ coefficients on the top and bottom surfaces of 100[1/m] and 500[1/m], respectively. The flat plate mesh with insulated boundary conditions on the sides was used to isolate through-the-thickness effects. Resulting temperature profiles at the surface and center of the laminate are shown in Figure (12). The higher $(h/k)_{eff}$ coefficient permits a more rapid transfer of heat into the laminate, causing the laminate to heat up and cure faster. This also allows more heat to escape from the laminate during the exotherm, resulting in an overall lower exotherm.

Corresponding degree of cure profiles, shown in Figure (13), demonstrate the significant influence $(h/k)_{eff}$ can have on the curing process. Lower $(h/k)_{eff}$ increases degree of cure gradients during the exotherm. The effective heat transfer across the laminate surface plays an important role in the development of residual stress and warpage during processing [10].

4.5 Thickness Effects

The thickness of the laminate will strongly influence the curing process. The effect of increasing laminate thickness on the temperature and degree of cure profiles is examined in glass/polyester laminates between 1.38 cm and 5.08 cm thick. Flat plate mesh geometries of similar nodal density to the flat plate mesh illustrated in Figure (5) were employed. Prescribed temperature boundary conditions defined by the glass/polyester cure cycle temperature history illustrated in Figure (11) were imposed on the top and bottom laminate surfaces. Insulated boundary conditions were enforced on the sides to isolate through-the-thickness processing effects. Predicted centerline temperature and degree of cure profiles are illustrated in Figures (14) and (15), respectively.

Temperature distributions at 164 minutes into the cycle, shown in Figure (16), demonstrate that while the 2.54 cm and thinner laminates are exotherming, the 5.08 laminate is still heating up at this point in the cycle. Similar gradients in the degree of cure distributions at 164 minutes are shown in Figure (17). The degree of cure gradients are most severe at this point in the 2.54 cm laminate. The interior of the 2.54 cm laminate is essentially cured. In contrast, the 5.08 cm laminate is essentially uncured at the interior. At a later point in the cure cycle, the thicker laminate will exotherm and its distributions will reverse shape similar to the thinner laminates, ultimately developing more
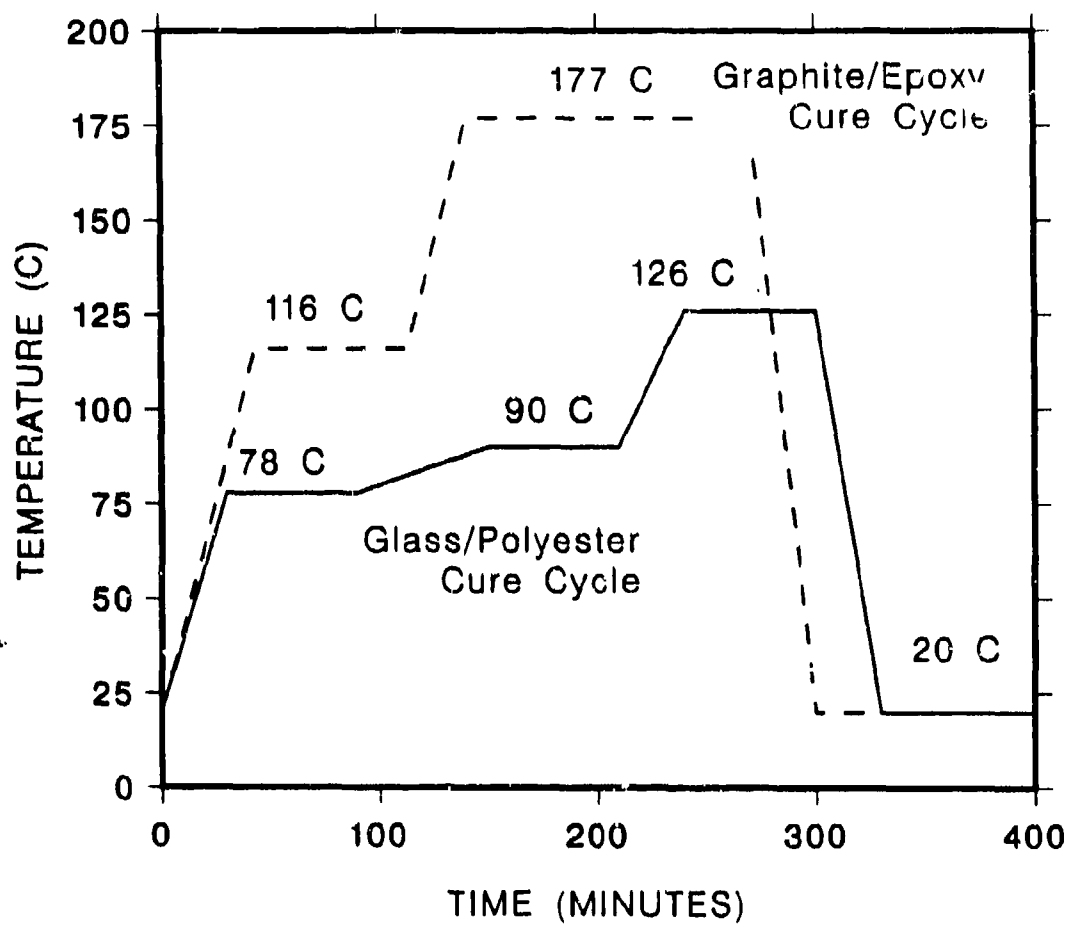
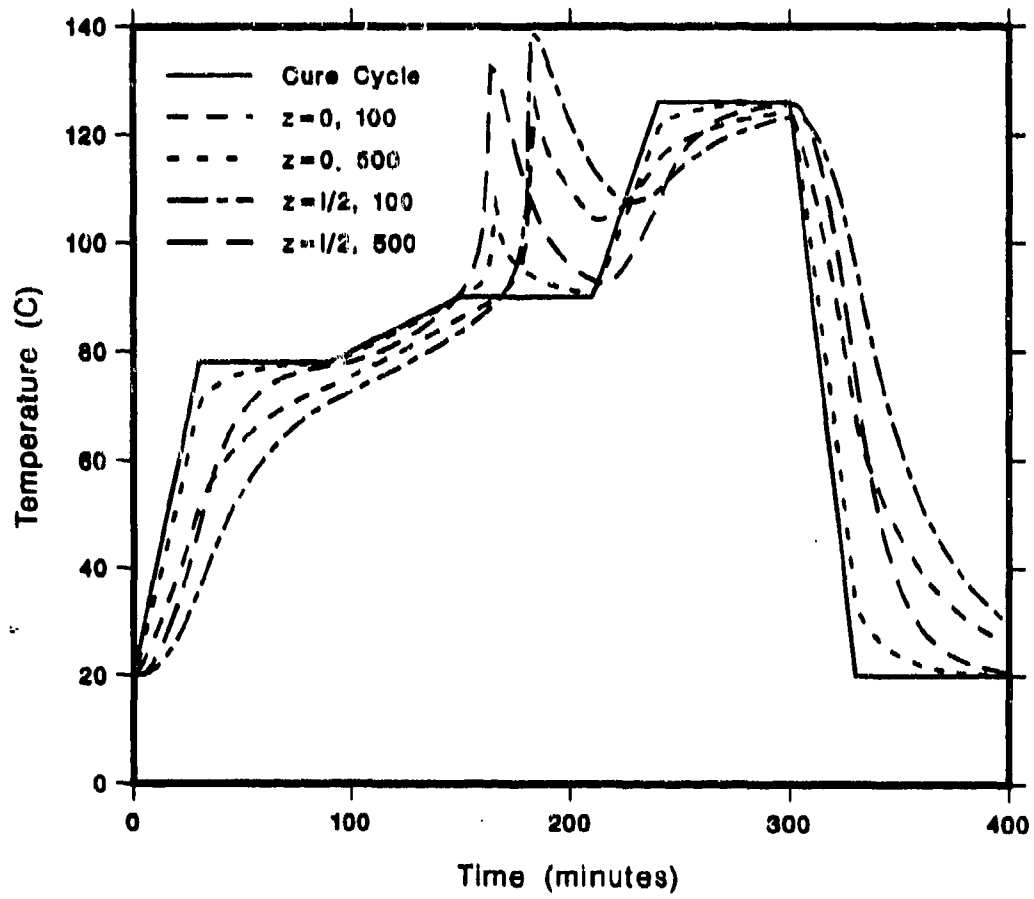Figure 11: Typical Glass/Polyester and Graphite/Epoxy Temperature Cure Cycles

29

Figure 12: Influence of $(h/k)_{eff}$ on Temperature Profiles in a Glass/Polyester Laminate
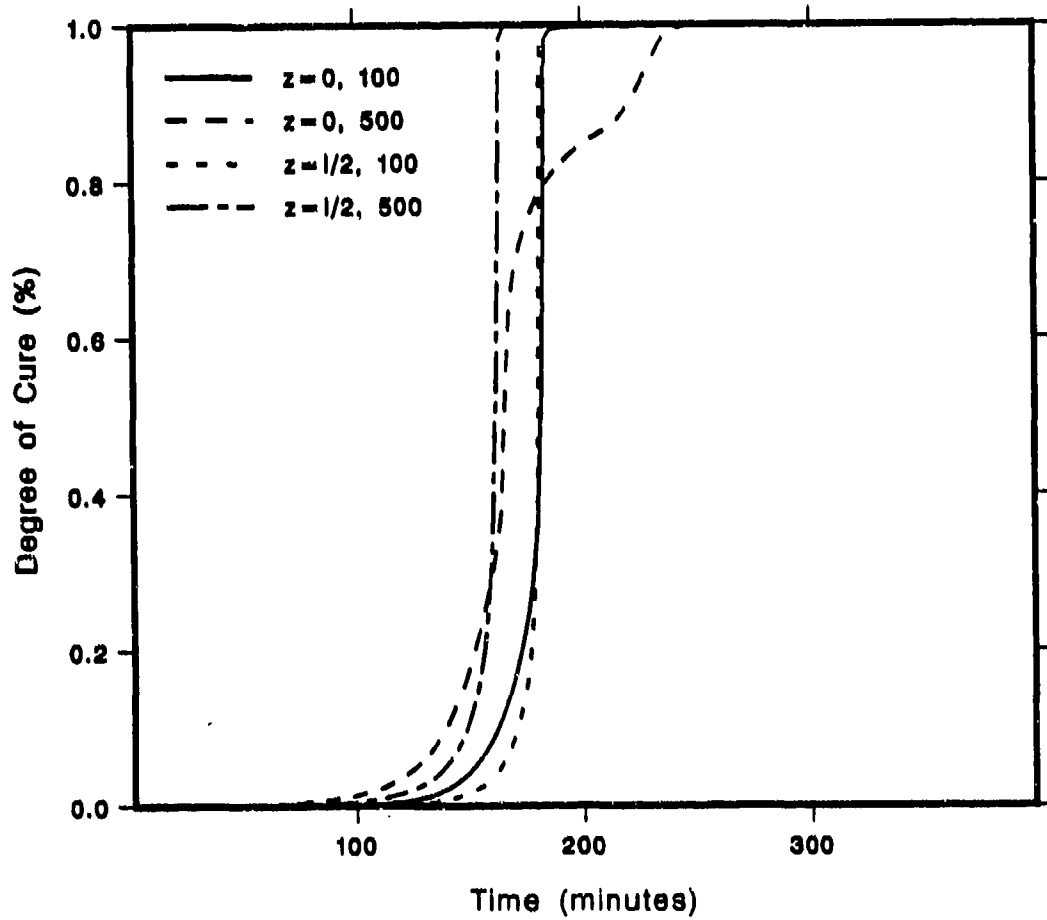
Figure 13: Influence of $(h/k)_{eff}$ on Degree of Cure Profiles in a Glass/Polyester Laminate
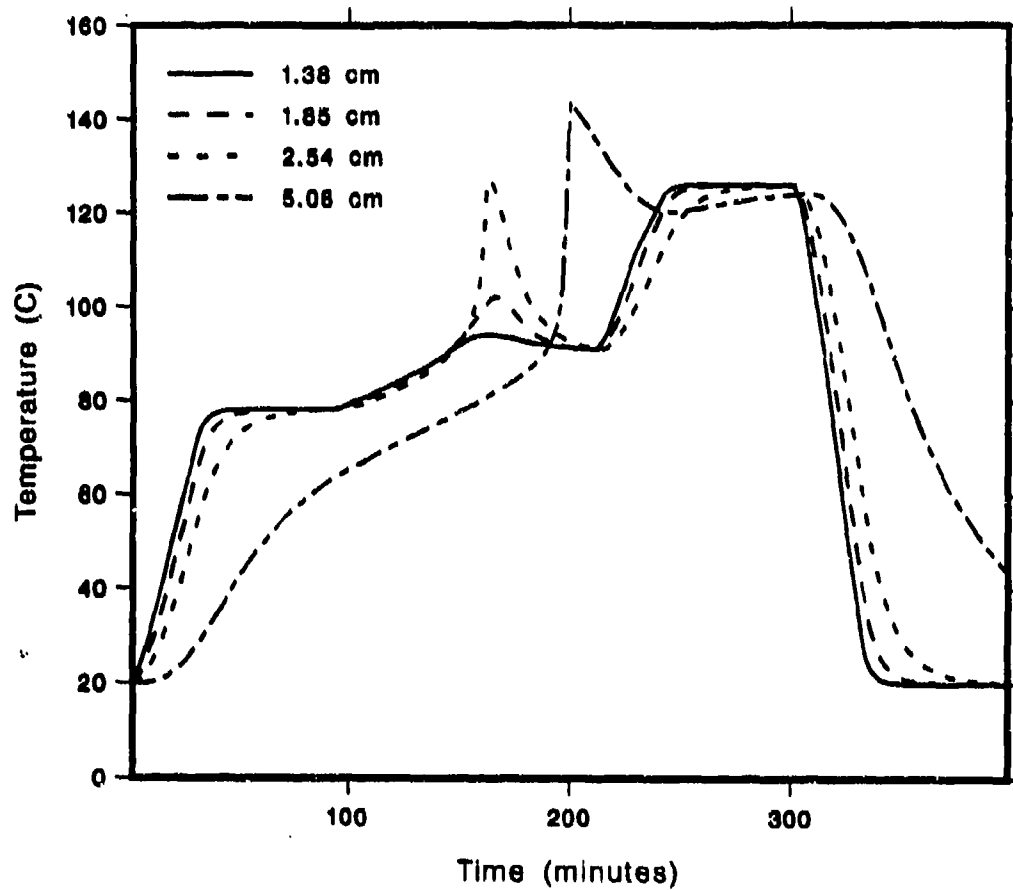
31

Figure 14: Influence of Thickness on Centerline Temperature Profiles in Glass/Polyester Laminates
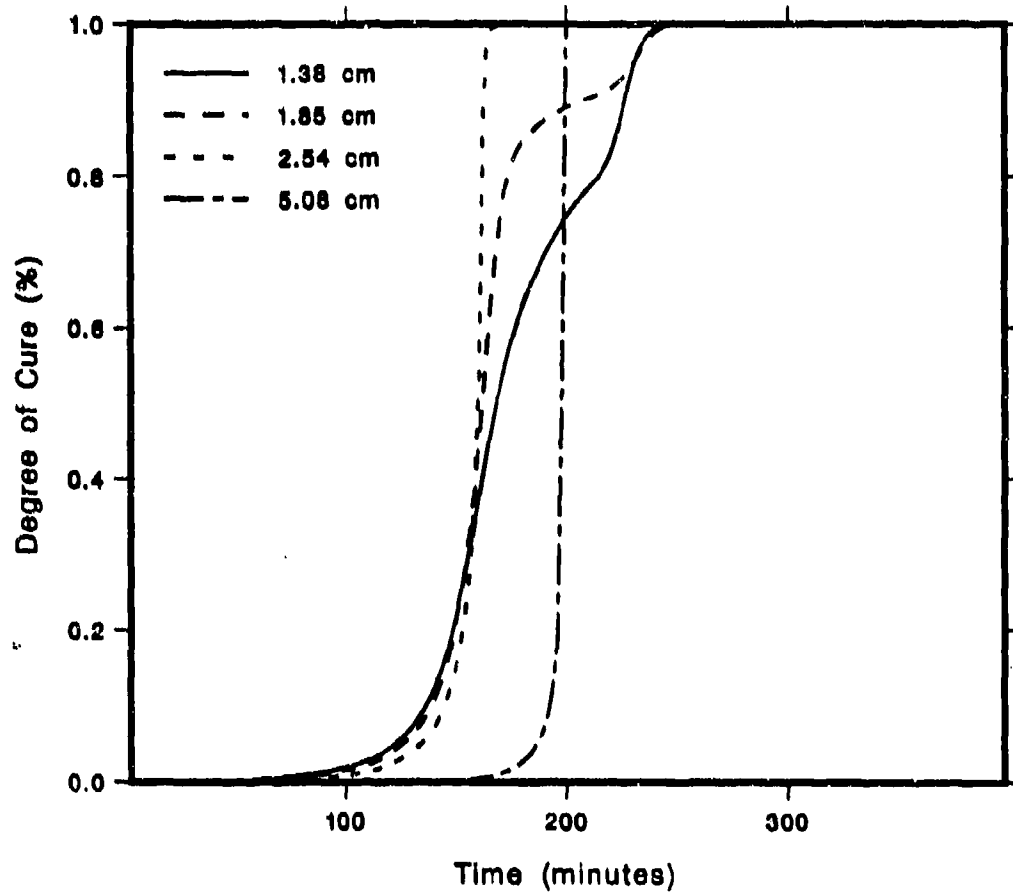
32

Figure 15: Influence of Thickness on Centerline Degree of Cure Profiles in Glass/Polyester Laminates

33

severe gradients. These results demonstrate the complex temperature and degree of cure gradients, unique to thick-sections, which develop during the curing process. Bogetti and Gillespie [10] have shown that these gradients have a profound influence on the evolution of process-induced stress and deformation.

4.6 Cure Cycle Temperature Ramp Effects

The cure cycle temperature ramp can strongly influence the temperature and degree of cure gradients that develop during the cure. The effect of the temperature cure cycle ramp on the degree of cure gradients is examined in a 2.54 cm glass/polyester laminate exposed to various cure cycle temperature ramps. The flat plate mesh with specified temperature boundary conditions on the top and bottom surfaces and insulated boundary conditions on the sides is used here. The laminate was cured at 80°C for 180 minutes before being subjected to temperature cure cycle ramps of 0.0, 0.25, 0.5 and 1.0 °C/min., illustrated in Figure (18). Predicted values of the degree of cure at the centerline minus the degree of cure on the surface of the laminate, $(\alpha_c - \alpha_s)$, are plotted in Figure (19) as a function of cycle time for the various temperature ramps investigated.

With this particular laminate thickness, 2.54 cm, the isothermal cure under the 0.0[°C/min.] ramp reveals a steadily increasing positive value of $(\alpha_c - \alpha_s)$, typical of an internal exotherm. Above a critical temperature ramp, the surface temperature rises relative to the interior since heat transfer by diffusion is low. Consequently, the surface temperature initiates the cure reaction. The exothermic reaction accelerates the cure and as a result creates a solidification front that sweeps the laminate from the outside towards the interior of the laminate. Curing from the outside to the inside may potentially entrap voids and volatile by-products of the chemical reaction and enhance warpage and residual stress development. Consequently, the temperature ramp can significantly influence the quality and in-service performance of the part.

4.7 Anisotropic Curing in Complex Shaped Composites

The anisotropic curing process in arbitrary shaped geometries is now presented to build another level of complexity in the cure simulation that enables realistic composite structures to be modeled.
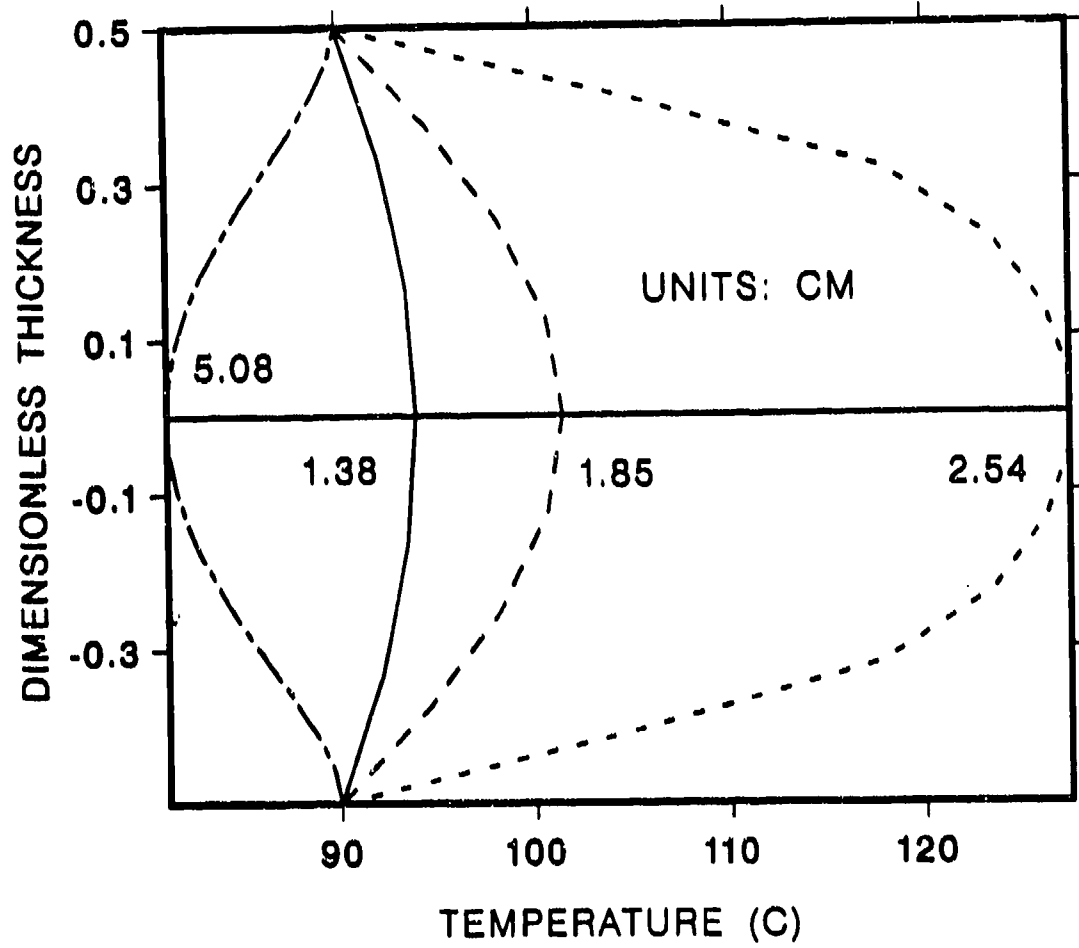
34

Figure 16: Temperatute Distributions in Glass/Polyester Laminates at Exotherm
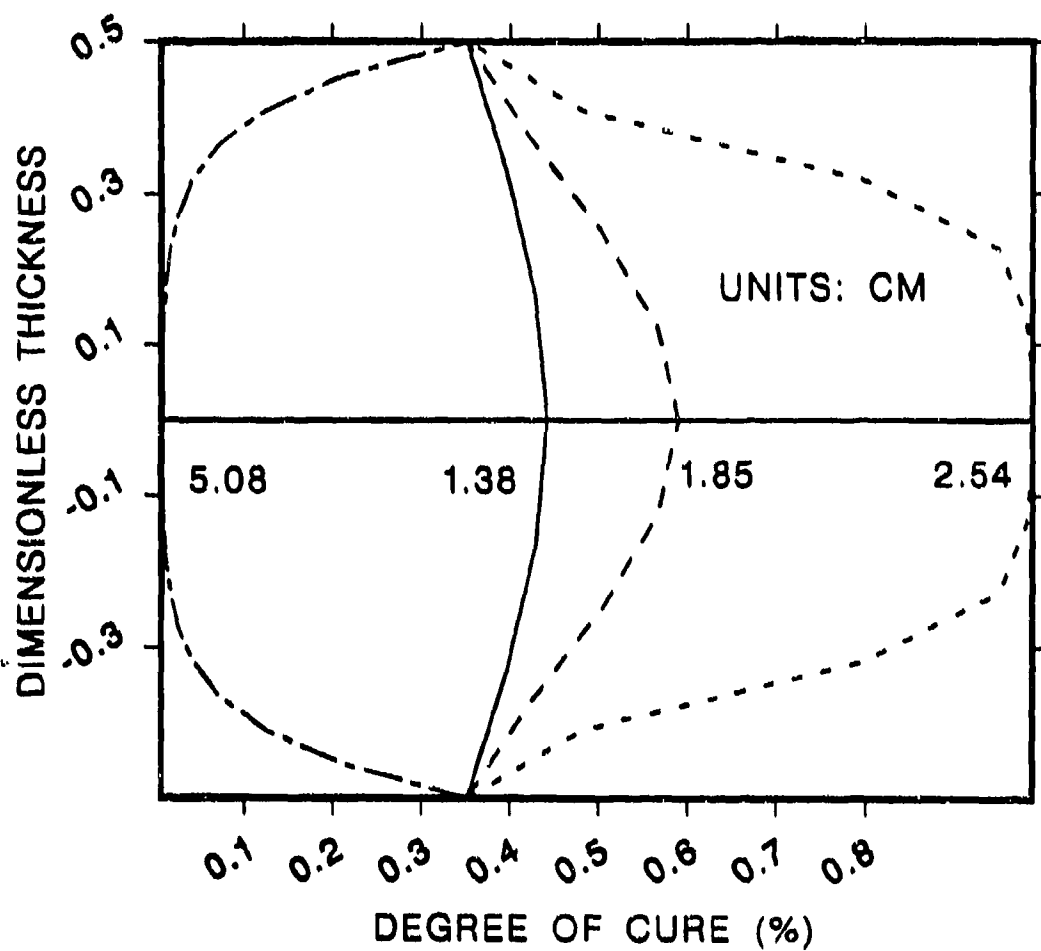
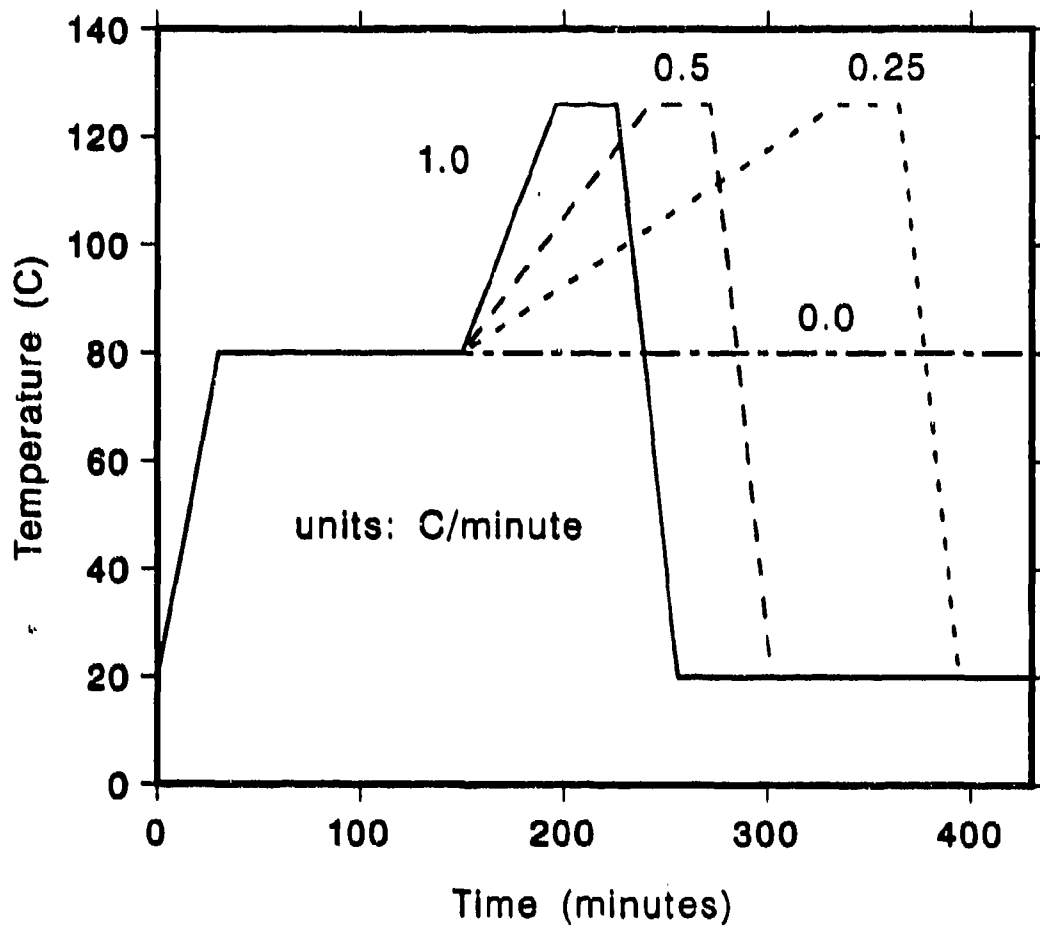Figure 17: Degree of Cure Distributions in Glass/Polyester Laminates at Exotherm

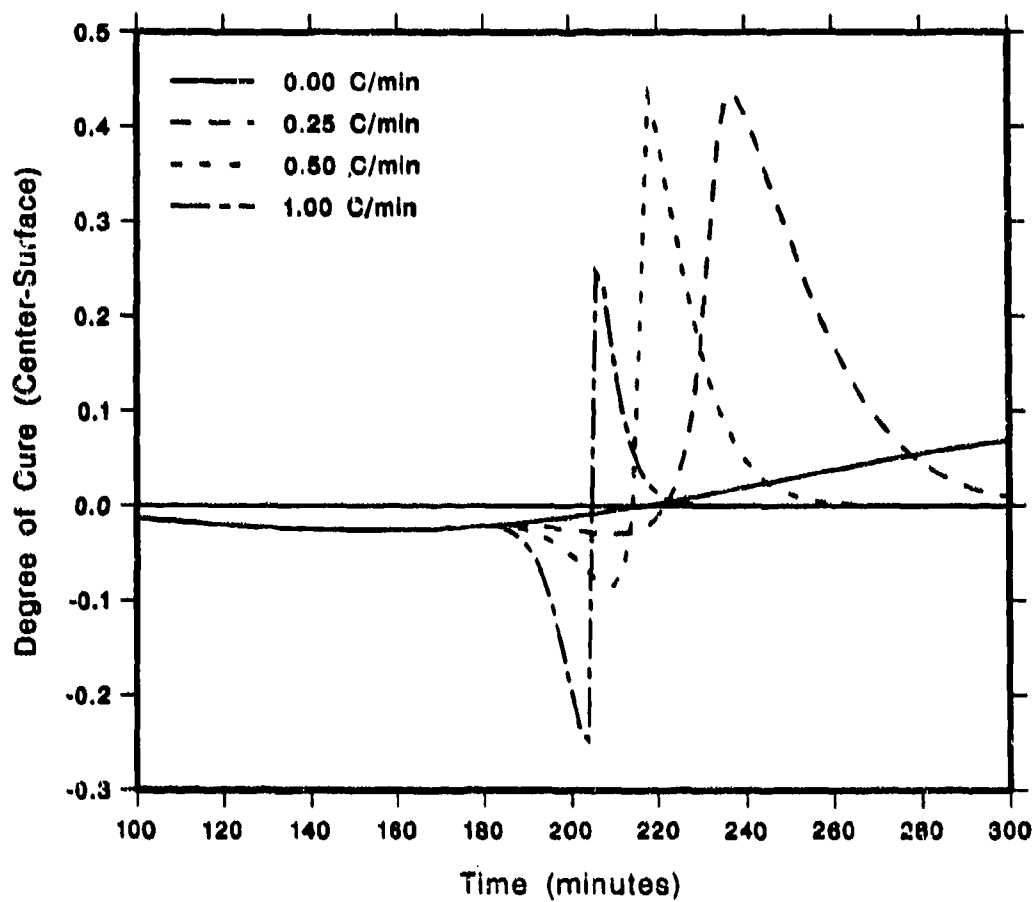Figure 18: Autoclave Temperature Cure Cycle Ramps

37

Figure 19: Effect of the Temperature Ramp on Non-uniform Curing in a 2.54 cm Glass/Polyester Laminate

The effect of anisotropic heat transfer on the curing process in a 2.54 cm thick 90° right angle bend graphite/epoxy structural element is examined. The angle bend mesh depicted in Figure (5) is used. A specified boundary condition defined by the graphite/epoxy cure cycle temperature history illustrated in Figure (11) was imposed on all four sides of the part. k_{11}/k_{33} ratios of 1, 5 and 10, typical of graphite/epoxy composites, were investigated.

Temperature contours are shown in Figure (20) at 145 minutes into the cure cycle, when the maximum exotherm occurs. The isotropic case, $k_{11}/k_{33} = 1$, exhibits through-the-thickness temperature gradients resembling a one-dimensional curing process. In contrast, k_{11}/k_{33} ratios of 5 and 10 demonstrate that temperature gradients at the bend are most severe at the inner radius and are accentuated by increased thermal anisotropy. This simulation clearly illustrates the significance of the anisotropic two-dimensional formulation used in our cure simulation analysis.

The curing process within a glass/polyester 90° right angle bend part is also examined. A k_{11}/k_{33} ratio of 2 is assumed in the simulation. Prescribed temperature boundary conditions defined in Figure (21) are imposed on all four sides of the part. This cure cycle is similar to the glass/polyester cycle defined in Figure (11) except the intermediate temperature ramp to 90°C is omitted.

Temperature and degree of cure contours at the time of maximum exotherm (165 minutes into the cycle) are illustrated in Figure (22). The complex temperature gradients indicate "hot" regions in each arm of the part geometry, moving inward towards the bend as they follow a sweeping cure front. The exotherm here is occurring on the outer regions of the part, sweeping toward the interior. The degree of cure contour at this point in the cycle indicates an outside to inside curing process. Severe gradients are noted with the surface fully cured and the interior uncured. This curing process will inevitably entrap any voids or chemical by-products, result in incomplete consolidation and potentially induce severe stress and deformation in the part during the curing process.

A final example examines the cure of a thick-section glass/polyester ply-drop structural element illustrated in Figure (5). Prescribed temperature boundary conditions defined in Figure (21) are imposed on the top and bottom surfaces while insulated conditions are imposed on the sides. A k_{11}/k_{33} of 2 is used. Temperature and degree of cure contours at the time of maximum exotherm
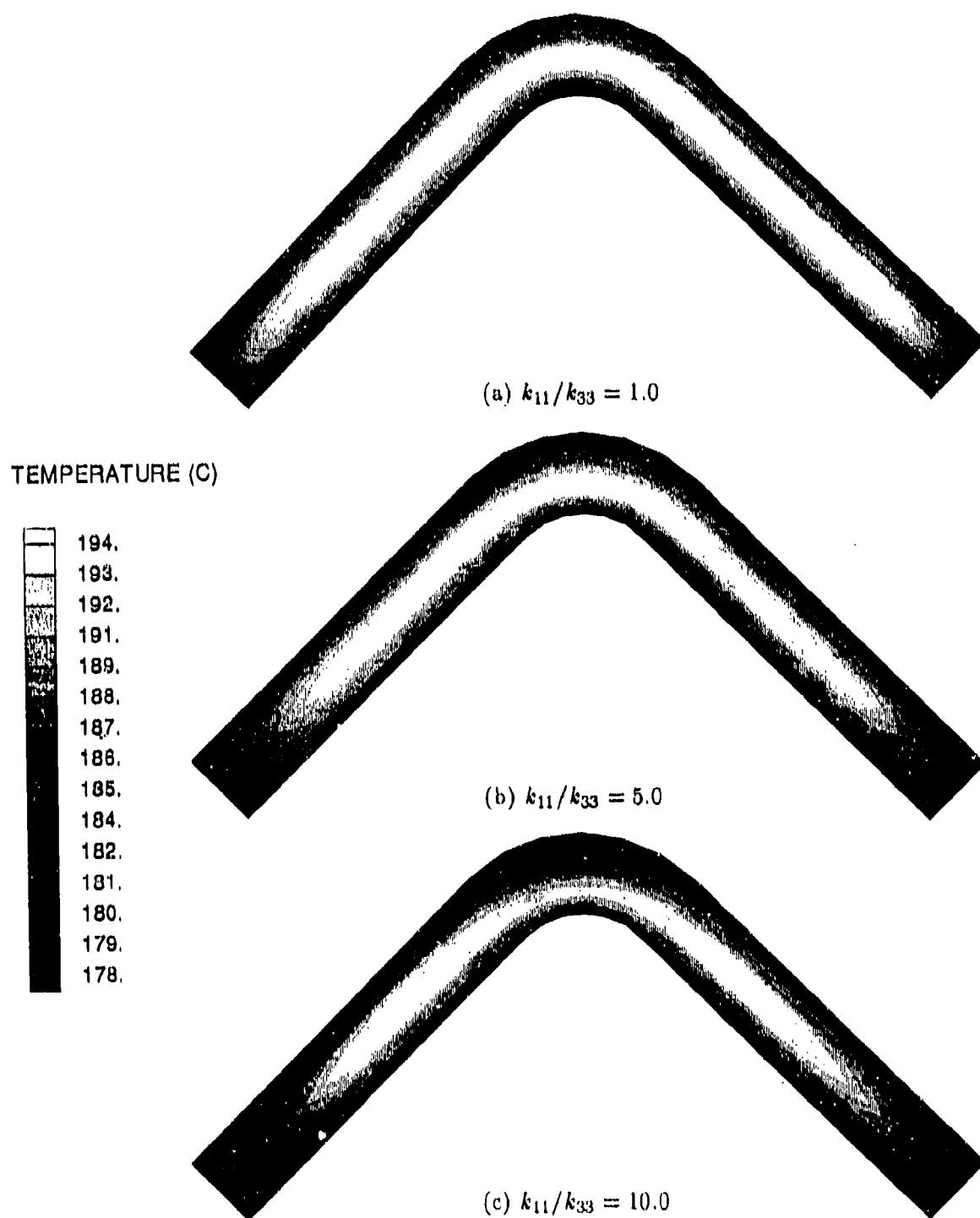
(a) $k_{11}/k_{33} = 1.0$

TEMPERATURE (C)

194.
193.
192.
191.
189.
188.
187.
186.
185.
184.
182.
181.
180.
179.
178.

(b) $k_{11}/k_{33} = 5.0$

(c) $k_{11}/k_{33} = 10.0$

Figure 20: Temperature Contours at Exotherm in a 2.54 cm Thick Graphite/Epoxy 90° Right Angle Bend

40
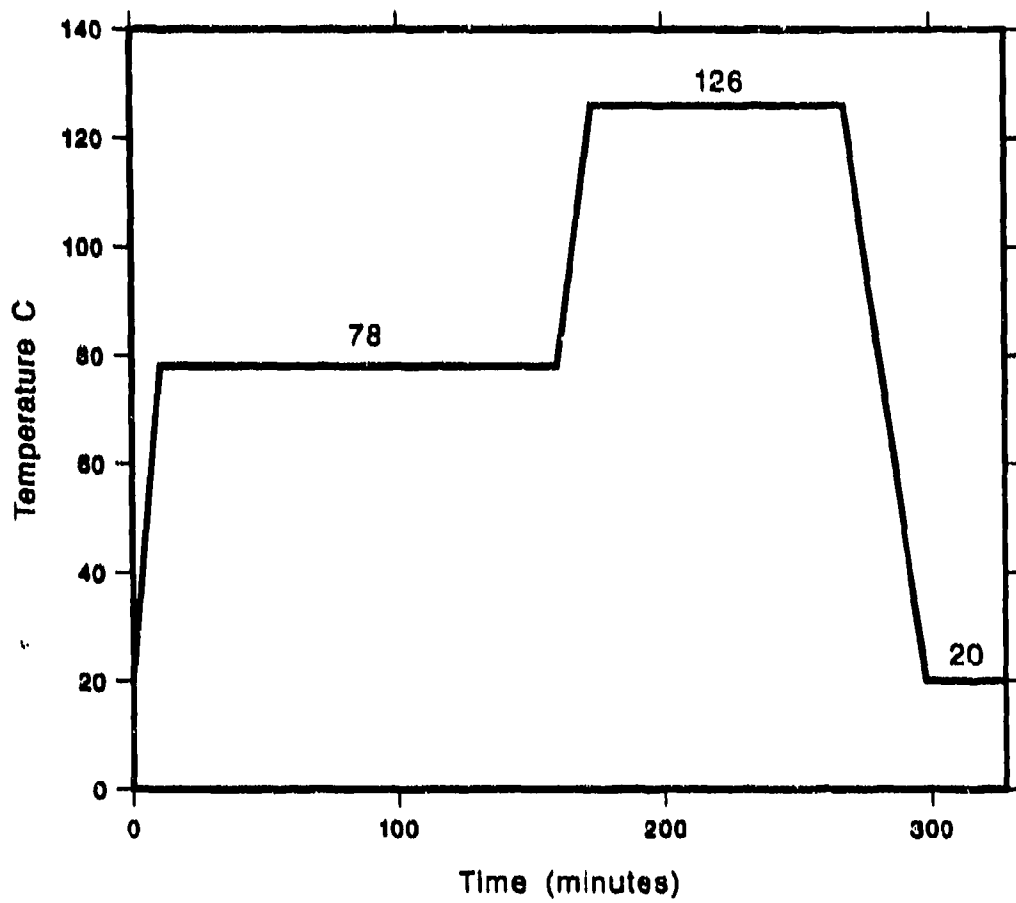
Figure 21: Condensed Glass/Polyester Cure Cycle
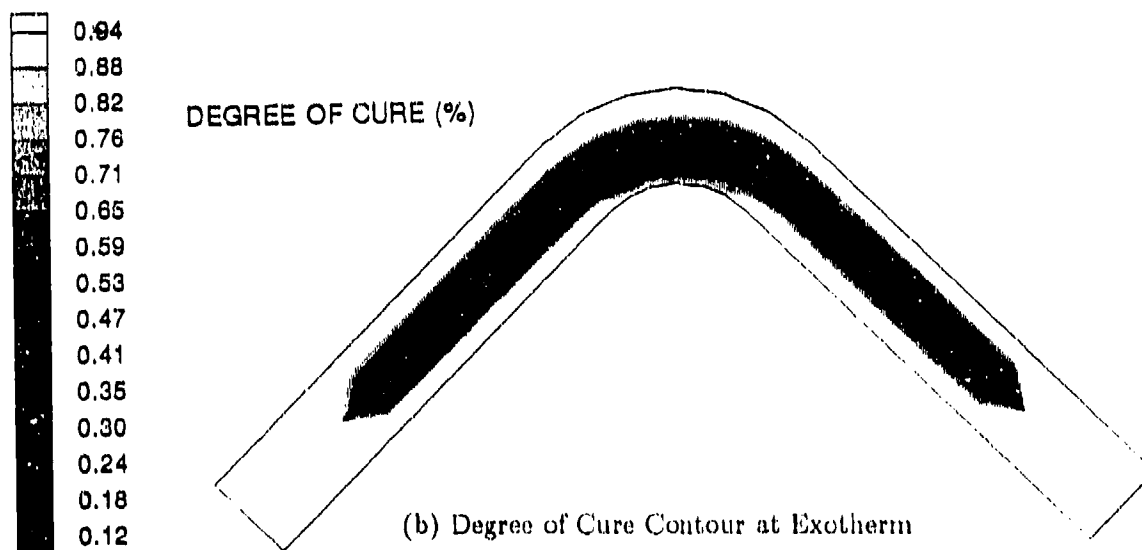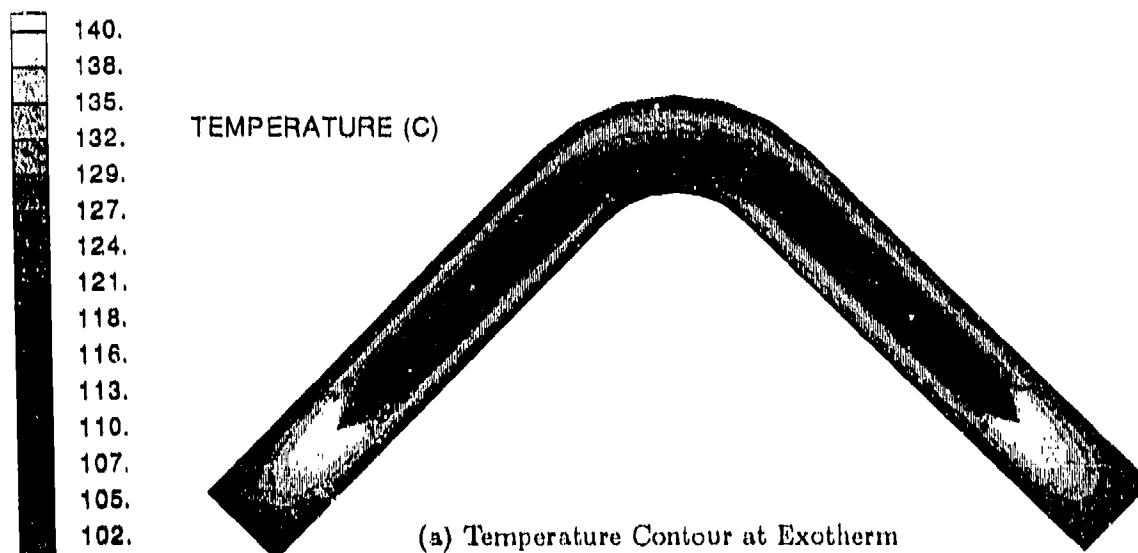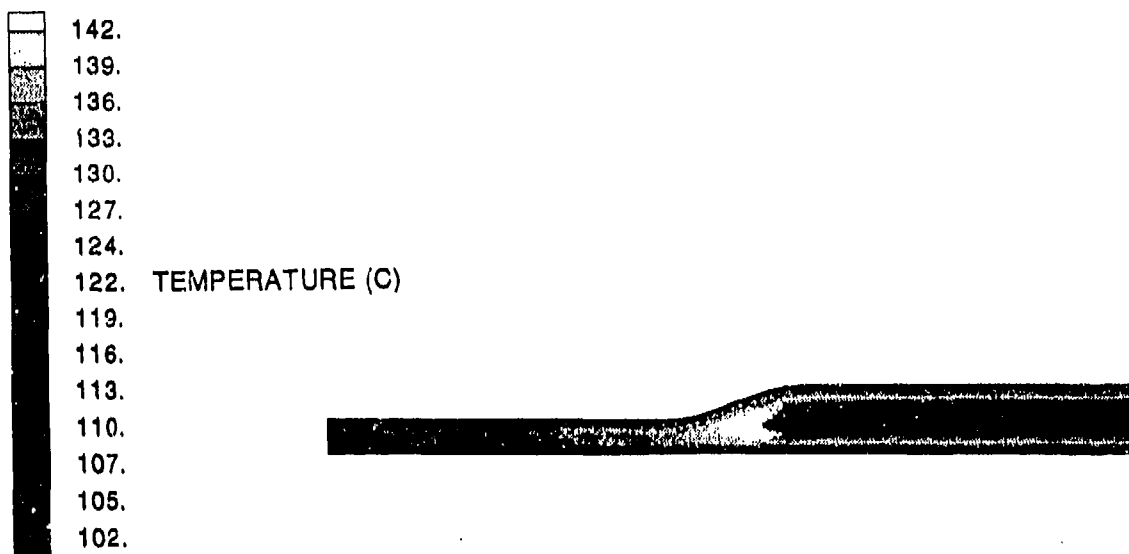
41

TEMPERATURE (C)

140.
138.
135.
132.
129.
127.
124.
121.
118.
116.
113.
110.
107.
105.
102.

(a) Temperature Contour at Exotherm

DEGREE OF CURE (%)

0.94
0.88
0.82
0.76
0.71
0.65
0.59
0.53
0.47
0.41
0.35
0.30
0.24
0.18
0.12

(b) Degree of Cure Contour at Exotherm

Figure 22: Anisotropic Curing in a 2.54 cm Thick Glass/Polyester 90° Right Angle Bend

42

(174 minutes) are presented in Figure (23). The results identify a "hot" region in the transition area with temperatures exceeding the autoclave by 45°C. The minimum temperature occurs within the interior of the thicker section. The corresponding degree of cure contour indicates severe gradients in the thicker section where the exterior region is fully cured and the interior is only 12% cured. In contrast, the thinner section of the ply-drop is completely cured at this portion of the process. The cure front is effectively sweeping from the thin section to the thick section.

The examples presented in this investigation clearly demonstrate the complex cure behavior encountered in the manufacture of thick-section thermoset structural components. Complex temperature and degree of cure gradients, accentuated by part geometry and anisotropic heat transfer, demonstrate the significant contribution made towards the processing science of thick-section thermosets. The cure simulation analysis developed here provides the detailed prerequiste information needed for predicting process-induced stress and deformation in thick-sections of arbitrary cross-section. This achievement represents a critical step in our ultimate goal of optimizing the quality and in-service performance of thermosetting structural components during the manufacturing process.

5 Conclusions

A two-dimensional anisotropic cure simulation analysis was developed to study the complex curing process within thick thermosetting composites of arbitrary cross-section. Complex gradients in temperature and degree of cure were predicted as a function of the autoclave temperature history and the influence of the tool on the curing process was demonstrated. Several typical glass/polyester and graphite/epoxy structural elements of arbitrary cross-section were analyzed to provide insight into the non-uniform curing process unique to thick-sections. Spatial gradients in degree of cure are shown to be strongly dependent on part geometry, thermal anisotropy, cure kinetics and the autoclave temperature cure cycle. These spatial gradients directly influence the quality and in-service performance of the finished component by inducing warpage and residual stress during the curing process. This work, therefore, represents an important step towards achieving our ultimate goal of building in quality, long life, predictable and reliable performance, durability and lower

43

142.
139.
136.
133.
130.
127.
124.
122. TEMPERATURE (C)
119.
116.
113.
110.
107.
105.
102.

(a) Temperature Contour at Exotherm

0.94
0.89
0.84
0.78
0.73
0.67
0.62
0.56 DEGREE OF CURE (%)
0.51
0.45
0.40
0.34
0.29
0.23
0.18
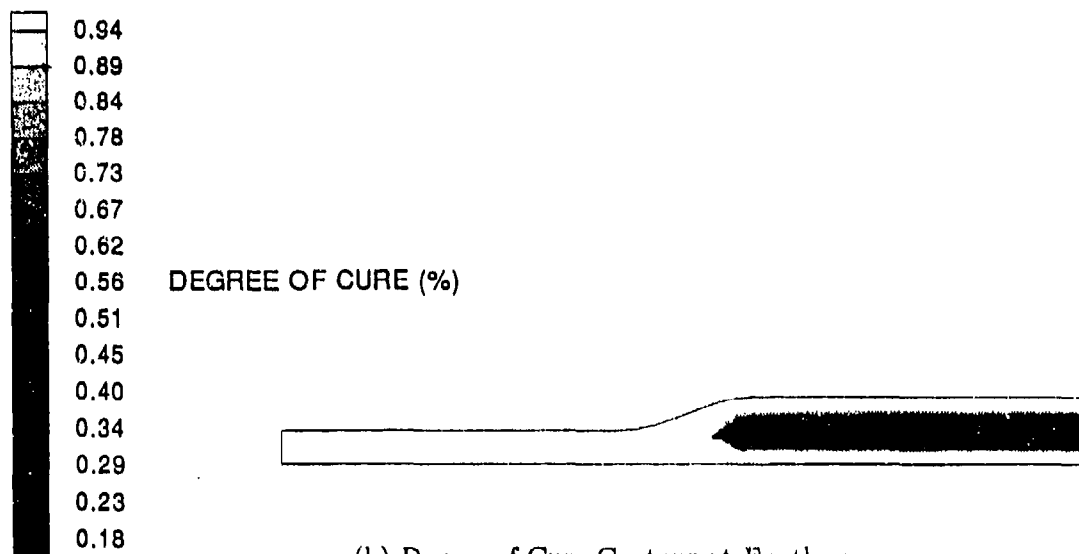
(b) Degree of Cure Contour at Exotherm

Figure 23: Anisotropic Curing in a Thick Glass/Polyester Ply-Drop

44

cycle costs of thick-section thermosetting composite structures for future Army systems.

INTENTIONALLY LEFT BLANK.

References

[1] Hahn, H.T. and Pagano, N.J. Curing stresses in composite laminates. *Journal of Composite Materials*, 9:91–105, 1975.

[2] Hahn, H.T. Residual stresses in polymer matrix composite laminates. *Journal of Composite Materials*, 10:266–277, 1976.

[3] Griffin, O.H. Three-dimensional curing stresses in symmetric cross-ply laminates with temperature-dependent properties. *Journal of Composite Materials*, 17:449–463, 1983.

[4] Stango, R.J. and Wang, S.S. Process-induced residual thermal stresses in advanced fiber-reinforced composite laminates. *Journal of Engineering for Industry*, 106:48–54, 1984.

[5] Kau, H. and Petrusha, L.A. Dimensional stability and property gradients in thick smc sections. Technical Report GMR-6359, General Motors Research Laboratories, Warren Michigan, 1988.

[6] Kays, A. O. Exploratory development on processing science of thick section composites. Technical Report AFWAL-TR-85-4090, Air Force Wright Aeronautical Laboratories, Wright Patterson AFB, Ohio, 1985.

[7] Dickerson, G. E. Fabrication of thick laminates. Technical Report LAR-12019, NASA Tech Brief, U.S. Patent No. 4,065,340.

[8] Meade, L. E. Fabrication of thick graphite/epoxy wing surface structures. In *24th National SAMPE Symposium and Exibition, Book 1*, 1979.

[9] Levitsky, M. and Shaffer, B.W. The approximation of temperature distributions in homogeneous exothermic reactions. *The Chemical Engineering Journal*, 5:235–242, 1973.

[10] Bogetti, T.A. and Gillespie, Jr., J. W. Process-induced stress and deformation in thick-section thermosetting composite laminates. In *21st SAMPE Technical Conference*, Atlantic City, N.J., September, 1989.

[11] McGee, S. H. Curing of particulate filled composites. *Polymer Engineering and Science*, 22:484, 1982.

[12] Loos, A. C. and Springer, G. S. Curing of epoxy matrix composites. *Journal of Composite Materials*, 17:135–169, 1983.

[13] Woo, I. L., Ciriscioli, P. R., Dusi, M. R., and Peterson, D. R. Cure process model of organic matrix composites in the presence of vapor release. *Journal of Reinforced Plastics and Composites*, 5:3–8, 1986.

[14] Cambell, F. C., Mallow, A. R., Amuedo, K. C., and Blase, G. A. Computer-aided curing of composites. Technical Report IR-0355-5, McDonnell Douglas Corporation, 1985.

[15] Woo, I. L. and Springer, G. S. Microwave curing of composites. *Journal of Composite Materials*, 18:387–409, 1984.

[16] Dave, R., Kardos, J. L., and Dudukovic, M. P. Process modeling of thermosetting matrix composites: A guide for autoclave cure cycle selection. In *Proceedings of the American Society for Composites First Technical Conference*, pages 137–153, Dayton, Ohio, 1986.

[17] Mallow, A. R., Muncaster, F. R., and Campbell, F. C. Science based cure model for composites. In *Proceedings of the American Society for Composites First Technical Conference*, pages 171–186, Dayton, Ohio, 1986.

[18] Springer, G. S. Resin flow during the cure of fiber reinforced composites. *Journal of Composite Materials*, 16:400–410, 1982.

[19] Levitsky, M. and Shaffer, B.W. Thermal stresses in chemically hardening elastic media with application to the molding process. *Journal of Applied Mechanics*, pages 647–651, September 1974.

[20] Shaffer, B.W. and Levitsky, M. Thermoelastic constitutive equations for chemically hardening materials. *Journal of Applied Mechanics*, pages 652–657, September 1974.

[21] Levitsky, M. and Shaffer, B.W. Residual thermal stresses in a solid sphere cast from a thermosetting material. *Journal of Applied Mechanics*, pages 651–655, September 1975.

[22] Özisik Necati M. *Heat Conduction*. Wiley Interscience, 1980.

[23] Morgan, R. J., Walkup, C. M., and Hoheisel, T. H. Characterization of the cure of carbon fiber/exopy composite prepregs by differential scanning calorimetry. *Journal of Composites Technology and Research*, 7:17–19, 1985.

[24] Adams, D.C. Cure behavior of unsaturated polyester resin composites. Technical Report CCM-88-16, Center for Composite Materials, University of Delaware, Newark, Delaware, 1988.

[25] Thompson, J. F., Thames, F. C., and Mastin, C. W. Automatic numerical generation of body-fitted curvilinear coordinate system for field containing any number of arbitrary two-dimensional bodies. *Journal of Computational Physics*, 15:299–319, 1974.

[26] Thompson, J. F., Waris, Z. A. U., and Mastin, C. W. Body-fitted coordinate systems for numerical solution of partial differential equations - a review. *Journal of Computational Physics*, 47:1–108, 1982.

[27] Gilmore, S. Tgmesh user's manual. Technical Report in press, Center for Composite Materials, University of Delaware, Newark, Delaware, 1989.

[28] Trafford, D. Computational analysis and simulation of the mold filling process for hele-shhaw flows. Technical Report CAE Report-3/86, Department of Mechanical and Aerospace Engineering, University of Delaware, Newark, Delaware, 1986.

[29] Barakat, H. Z. and Clark, J. A. On the solution of the diffusion equations by numerical methods. *Journal of Heat Transfer*, pages 421–427, 1966.

INTENTIONALLY LEFT BLANK.

A Appendix

A.1 Finite Difference Approximations

Finite difference approximations to the partial derivatives used in the analysis are presented below. In the following formulas, the temperature, T, and the spatial coordinates, x and z, are represented symbolically as f. In addition, subscripts η and ξ denote partial differentiation with respect to the computational coordinates and the subscripts i and j refer to the nodal location on the computational grid. Both central and one-sided differencing expressions are utilized.

A.1.1 Central Differencing

Three-point central differencing formulas are used at the interior nodes of the discretized domain. The first order derivatives are given by:

$$f_\xi = (f_{i+1,j} - f_{i-1,j})/2\Delta\xi \tag{21}$$

and

$$f_\eta = (f_{i,j+1} - f_{i,j-1})/2\Delta\eta \tag{22}$$

Second order derivatives are given by:

$$f_{\xi\xi} = (f_{i+1,j} - 2f_{i,j} + f_{i-1,j})/(\Delta\xi)^2 \tag{23}$$

and

$$f_{\eta\eta} = (f_{i,j+1} - 2f_{i,j} + f_{i,j-1})/(\Delta\eta)^2 \tag{24}$$

with the cross-term derivative:

$$f_{\xi\eta} = (f_{i+1,j+1} - f_{i-1,j+1} - f_{i+1,j-1} + f_{i-1,j-1})/4\Delta\xi\Delta\eta \tag{25}$$

A.1.2 One-Sided Differencing

The three-point one-sided differencing formulas used to represent the temperature gradients on the boundaries of the domain in the generalized boundary condition formulation are given below for

each face of the computational mesh. On the $(\xi = 1)$ face, the normal derivative is approximated by the forward differencing expression:

$$(f_\xi)_{i,j} = (-3f_{i,j} + 4f_{i+1,j} - f_{i+2,j})/\Delta\xi \tag{26}$$

and on the $(\xi = m)$ face by the backward differencing expression:

$$(f_\xi)_{i,j} = (3f_{i,j} - 4f_{i-1,j} - f_{i-2,j})/\Delta\xi \tag{27}$$

On the $(\eta = 1)$ face, the normal derivative is approximated by the forward differencing expression:

$$(f_\eta)_{i,j} = (-3f_{i,j} + 4f_{i,j+1} - f_{i,j+2})/\Delta\eta \tag{28}$$

and on the $(\eta = n)$ face by the backward differencing expression:

$$(f_\eta)_{i,j} = (3f_{i,j} - 4f_{i,j-1} - f_{i,j-2})/\Delta\xi \tag{29}$$

$\Delta\xi$ and $\Delta\eta$ are identically 1 in the computational domain.

A.1.3 Explicit Time Differencing Formula

The explicit finite difference approximation for the time derivative of temperature is given by:

$$\frac{\partial T}{\partial t} = (T_{i,j}^{t+\Delta t} - T_{i,j}^{t})/\Delta t \tag{30}$$

A.2 Boundary-Fitted Coordinate System Transformation Coefficients

The coefficients contained in the transformed governing equation and generalized boundary condition are listed below. Derivatives on the physical domain coordinates, x and z, with respect to ξ and η are presented above.

A.2.1 Governing Equation Coefficients

The A_i coefficients appearing in the transformed governing equation are given by:

$$A_1 = (k_{xx}z_\eta^2 - 2k_{xz}x_\eta z_\eta + k_{zz}x_\eta^2)/J^2 \tag{31}$$

52

$$A_2 = (k_{xx}z_\xi^2 - 2k_{xz}x_\xi z_\xi + k_{zz}x_\xi^2)/J^2 \tag{32}$$

$$A_3 = (-2k_{xx}z_\eta z_\xi - 2k_{zz}x_\eta x_\xi + 2k_{xz}(x_\xi z_\eta + x_\eta z_\xi)))/J^2 \tag{33}$$

$$A_4 = (k_{xx}C_1 + k_{zz}C_2 + 2k_{xz}C_3)/J^2 \tag{34}$$

$$A_5 = (k_{xx}C_4 + k_{zz}C_5 + 2k_{xz}C_6)/J^2 \tag{35}$$

with the coefficients C_i given by:

$$C_1 = z_\eta z_{\xi\eta} - z_\xi z_{\eta\eta} + (z_\xi z_\eta J_\eta - z_\eta^2 J_\eta)/J \tag{36}$$

$$C_2 = x_\eta x_{\xi\eta} - x_\xi x_{\eta\eta} + (x_\xi x_\eta J_\eta - x_\eta^2 J_\eta)/J \tag{37}$$

$$C_3 = x_\xi z_{\eta\eta} - x_\eta z_{\xi\eta} + (x_\eta x_\eta J_\xi - x_\xi z_\eta J_\eta)/J \tag{38}$$

$$C_4 = z_\xi z_{\xi\eta} - z_\eta z_{\xi\xi} + (z_\xi z_\eta J_\xi - z_\xi^2 J_\eta)/J \tag{39}$$

$$C_5 = x_\xi x_{\xi\eta} - x_\eta x_{\xi\xi} + (x_\xi x_\eta J_\xi - x_\xi^2 J_\eta)/J \tag{40}$$

$$C_6 = x_\eta z_{\xi\xi} - x_\xi z_{\xi\eta} + (x_\xi z_\xi J_\eta - x_\eta z_\xi J_\xi)/J \tag{41}$$

The corresponding *Jacobians* appearing in the C_i expressions are given by:

$$J = x_\xi z_\eta - z_\xi x_\eta \tag{42}$$

$$J_\xi = x_{\xi\xi}z_\eta + x_\xi z_{\xi\eta} - x_{\xi\eta}z_\xi - x_\eta z_{\xi\xi} \tag{43}$$

$$J_\eta = x_{\xi\eta}z_\eta + x_\xi z_{\eta\eta} - x_{\eta\eta}z_\xi - x_\eta z_{\xi\eta} \tag{44}$$

A.2.2 Boundary Conditions Coefficients

The coefficients used in the normal direction temperature gradients are given by:

$$\alpha = x_\eta^2 + y_\eta^2 \tag{45}$$

$$\beta = x_\xi x_\eta + y_\eta y_\xi \tag{46}$$

$$\gamma = x_\xi^2 + y_\xi^2 \tag{47}$$

53

INTENTIONALLY LEFT BLANK.

56

No. of
Copies   Organization

2   FMC Corporation
         ATTN: Eric Weerth
         Manager, Advance Structures and
            Materials Dept.
         1105 Coleman Avenue, Box 1201
         San Jose, CA 95108

2   ARDEC CCAC
         ATTN: S. Mursalli
                J. Hederich
         Picatinny Arsenal, NJ 07806-5000

2   PM-TMAS
         Picatinny Arsenal, NJ 07806-5000

2   DARPA
         ATTN: J. Kelly
         1400 Wilson Blvd
         Arlington, VA 22209

Intentionally left blank.

USER EVALUATION SHEET/CHANGE OF ADDRESS

This Laboratory undertakes a continuing effort to improve the quality of the reports it publishes.
Your comments/answers to the items/questions below will aid us in our efforts.

1. BRL Report Number _____BRL-TR-3121_____ Date of Report _____July 1990_____.

2. Date Report Received _____

3. Does this report satisfy a need? (Comment on purpose, related project, or other area of interest
for which the report will be used.) _____
_____
_____

4. Specifically, how is the report being used? (Information source, design data, procedure, source
of ideas, etc.) _____
_____
_____

5. Has the information in this report led to any quantitative savings as far as man-hours or dollars
saved, operating costs avoided, or efficiencies achieved, etc? If so, please elaborate. _____
_____
_____

6. General Comments. What do you think should be changed to improve future reports? (Indicate
changes to organization, technical content, format, etc.) _____
_____
_____
_____

CURRENT
ADDRESS

Name _____

Organization _____

Address _____

City, State, Zip Code _____

7. If indicating a Change of Address or Address Correction, please provide the New or Correct
Address in Block 6 above and the Old or Incorrect address below.

OLD
ADDRESS

Name _____

Organization _____

Address _____

City, State, Zip Code _____

(Remove this sheet, fold as indicated, staple or tape closed, and mail.)